OPEN ACCESS

Original research

NFATc1 signaling drives chronic ER stress responses to promote NAFLD progression

Muhammad Umair Latif,[1] Geske Elisabeth Schmidt,[1] Sercan Mercan,[1] Raza Rahman,[2] Christine Silvia Gibhardt ,[3] Ioana Stejerean-Todoran ,[3] Kristina Reutlinger,[1] Elisabeth Hessmann,[1] Shiv K Singh ,[1] Abdul Moeed,[4] Abdul Rehman,[5] Umer Javed Butt,[6] Hanibal Bohnenberger,[7] Philipp Stroebel,[7] Sebastian Christopher Bremer ,[1] Albrecht Neesse ,[1] Ivan Bogeski,[3] Volker Ellenrieder [1]

► Additional supplemental material is published online only. To view, please visit the journal online (http://dx.doi.org/10.1136/gutjnl-2021-325013).

For numbered affiliations see end of article.

Correspondence to
Professor Volker Ellenrieder, Department of Gastroenterology, Gastrointestinal Oncology and Endocrinology, University Medical Center Göttingen, Gottingen, Niedersachsen, Germany;
volker.ellenrieder@med.uni-goettingen.de

Received 27 April 2021
Accepted 6 February 2022

To cite: Latif MU, Schmidt GE, Mercan S, *et al*. *Gut* Epub ahead of print: [*please include* Day Month Year]. doi:10.1136/gutjnl-2021-325013

ABSTRACT

Objectives Non-alcoholic fatty liver disease (NAFLD) can persist in the stage of simple hepatic steatosis or progress to steatohepatitis (NASH) with an increased risk for cirrhosis and cancer. We examined the mechanisms controlling the progression to severe NASH in order to develop future treatment strategies for this disease.

Design NFATc1 activation and regulation was examined in livers from patients with NAFLD, cultured and primary hepatocytes and in transgenic mice with differential hepatocyte-specific expression of the transcription factor (*Alb-cre, NFATc1*$^{c.a}$. and *NFATc1*$^{\Delta/\Delta}$). Animals were fed with high-fat western diet (WD) alone or in combination with tauroursodeoxycholic acid (TUDCA), a candidate drug for NAFLD treatment. NFATc1-dependent ER stress-responses, NLRP3 inflammasome activation and disease progression were assessed both in vitro and in vivo.

Results NFATc1 expression was weak in healthy livers but strongly induced in advanced NAFLD stages, where it correlates with liver enzyme values as well as hepatic inflammation and fibrosis. Moreover, high-fat WD increased NFATc1 expression, nuclear localisation and activation to promote NAFLD progression, whereas hepatocyte-specific depletion of the transcription factor can prevent mice from disease acceleration. Mechanistically, NFATc1 drives liver cell damage and inflammation through ER stress sensing and activation of the PERK-CHOP unfolded protein response (UPR). Finally, NFATc1-induced disease progression towards NASH can be blocked by TUDCA administration.

Conclusion NFATc1 stimulates NAFLD progression through chronic ER stress sensing and subsequent activation of terminal UPR signalling in hepatocytes. Interfering with ER stress-responses, for example, by TUDCA, protects fatty livers from progression towards manifest NASH.

Significance of this study

What is already known on this subject?
- Non-alcoholic fatty liver disease (NAFLD) is a major cause of chronic liver disease.
- Exposure to lipotoxic fatty acids can cause endoplasmic reticulum (ER) stress in hepatocytes.
- Chronic unresolved ER stress drives NAFLD progression.

What are the new findings?
- NFATc1 is highly activated in advanced NAFLD.
- Lipotoxic fatty acids stimulate NFATc1 expression, nuclear localisation and activation in hepatocytes.
- NFATc1 activation drives liver cell damage and inflammation through chronic ER stress sensing and activation of the terminal PERK-CHOP unfolded protein response (UPR) pathway.
- Inhibition of chronic ER stress responses by tauroursodeoxycholic acid (TUDCA) blocks NFATc1 mediated terminal UPR signalling and prevents NAFLD progression.

How might it impact on clinical practice in the foreseeable future?
- Our findings indicate a critical role of NFATc1 in chronic ER stress responses and NAFLD progression. Targeting unrestricted ER stress alleviates NFATc1-driven cell damage and therefore, our study provides the rational for current clinical trials aiming at the potential of TUDCA treatment in NAFLD.

INTRODUCTION

Non-alcoholic liver disease (NAFLD) is emerging as the leading cause of chronic liver disease with an estimated worldwide prevalence of more than 25%.[1 2] NAFLD is often associated with metabolic disorders, for example, insulin resistance, type-2 diabetes or obesity, and usually presents as simple hepatic steatosis (NAFL). However, in about 20%, the disease can progress to non-alcoholic steatohepatitis (NASH), which carries an increased risk of developing cirrhosis, liver failure and hepatocellular carcinoma.[3 4] In recent years, enormous efforts have been made to develop drug strategies for the treatment of NAFLD, but until now there are no approved drugs for the prevention or therapy of NASH in clinical use.

The lack of effective treatment is largely due to a still incomplete understanding of the molecular mechanisms responsible for the development and progression of the disease. Excessive accumulation of fatty acids and lipotoxic metabolites in hepatocytes is considered a key event in the initiation of NAFLD.[5–7] It has been shown, for example, that sustained exposure to lipotoxic fatty acids can cause hepatocyte cell damage via induction of chronic endoplasmic reticulum (ER) stress and subsequent activation of the terminal unfolded protein response (UPR) pathway. UPR in turn activates the NLRP3 multiprotein inflammasome complex to foster hepatocyte cell death and inflammation in response to unresolved ER stress.[7–10] Accordingly, high expression of NLRP3 inflammasome markers (NLRP3, Caspase-1, Caspase-11, interleukin (IL)-1β and IL-18) are found in liver biopsies from patients with NASH.[11 12] However, the endogenous pathways responsible for chronic ER stress sensing and NLRP3 activation in fatty liver remain largely unknown.

Nuclear factor of activated T cells (NFAT) proteins comprises a family of calcium responsive transcription factors (NFATc1-NFATc4) involved in the regulation of adaptive cellular functions within and outside the immune system.[12 13] Activation of NFAT proteins result in response to extracellular stimuli and in adaptation to multiple cellular stress signals. Moreover, ectopic activation of individual family members has been described in metabolic (eg, diabetes mellitus), inflammatory (eg, psoriasis) and malignant diseases (eg, pancreatic cancer and melanoma).[12 14–21] When inactive, NFAT proteins reside in the cytosol in a hyperphosphorylated state. Following accumulation of cytosolic calcium, NFAT proteins become dephosphorylated by the phosphatase calcineurin and shuttle into the nucleus, where they regulate target gene signatures in concert with other site-specific transcription factors and chromatin remodelling proteins.[12] Some recent investigations have reported higher NFAT expression and activation levels in chronic hepatitis and in liver cancer as well. It has been shown, for instance, that NFATc4 promotes PPARα expression in hepatocytes and stimulates liver fibrosis through activation of hepatic stellate cells.[22–24]

Here, we describe for the first time a causal role of NFATc1 in NAFLD progression. We show that NFATc1 fosters chronic ER stress sensing and cell damage responses via the NLRP3 inflammasome pathway. Furthermore, we provide experimental evidence that pharmacological interference with terminal ER stress responses may oppose NFATc1-driven progression of NAFLD.

MATERIALS AND METHODS

Human samples

Formalin-fixed, paraffin-embedded human tissues identified from patients with NASH were retrieved from the biobank of the Institute of Pathology, University Medical Center, Goettingen. Normal liver sections from patients with early steatosis were used as controls. All samples were used for immunohistochemical analysis of NFATc1 and analysed using imageJ software. Briefly, percentage of nuclear NFATc1 positive hepatocytes in 10 images per sample (Scale bar=50 µm) was calculated manually. NAFLD activity score (NAS) and degree of fibrosis were determined as described before.[25] NFATc1 expression in patients with NASH was correlated with the NAS, the degree of fibrosis and serum levels of liver enzymes (ALT and AST) by simple linear regression.

Animal model

All animal experiments were approved and carried out according to the regulations of Federation of European Laboratory Animal Science Associations (Laves approval No. 33.9-42502-04-16/2189 and 33.9-42502-04-14/1633). *Alb-Cre*, *NFATc1* and *NFATc1*$^{\Delta/\Delta}$ mice have been described previously.[19 26–28] The *c.a.NFATc1* knock-in strain was generated by cloning an N-terminal hemagglutinin (HA)-tagged constitutively active version of NFATc1 containing serine to alanine substitutions in the conserved serine-rich domain and all three serine-proline repeats into the ROSA26 promoter locus (Artemis Pharmaceuticals). The strains were interbred to generate *Alb-Cre;NFATc1*$^{\Delta/\Delta}$ and *Alb-Cre;NFATc1*$^{c.a}$. (hereafter referred to as *NFATc1*$^{\Delta/\Delta}$ and *NFATc1*$^{c.a}$., respectively) mice. All mice were genotyped by PCR as explained before.[19]

RNA-Seq

Total RNA was isolated from AML12 cells transfected with either HA-tagged c.n.NFATc1 or control plasmid. Purity and integrity of RNA samples were validated by gel electrophoresis. TruSeq RNA Library Prep Kits (RS-122-2001 and RS-122-2002) from Illumina were used to prepare libraries following instructions from manufacturer and sequencing was performed by NGS Integrative Genomics Core Unit, University Medical Center Goettingen, Germany.

Obtained FastQ files were analysed by using usegalaxy.eu,[29] FastQ files were analysed for quality control followed by mapping to murine transcriptome (mm9) using TopHat tool (V.2.1.1),[30] with very sensitive bowtie2 settings, followed by HTSeq (V.0.9.1; -f bam -r pos -s reverse -a 10 -t exon -m union).[31] Differential gene expression analysis was performed with DESeq2 (V.2.11.40.6),[32] as well as principal component analysis (PCA). Heat maps were generated in GraphPad prims V.7.0. NFATc1-dependent differentially expressed genes (log2fold values≥0.5/≤−0.5; p≤0.05; base mean>10) were analysed in reactome (reactome.org) pathway database.

Detailed description of animal treatments and further materials and methods is included in the online supplemental information.

RESULTS

Nuclear NFATc1 activation in progressive human and murine NAFLD

To assess NFATc1 expression and activation in NAFLD progression, we performed immunohistochemical analyses in tissue samples from patients with healthy liver (n=8) and progressive NAFLD (n=46). These studies revealed absent or weak NFATc1 expression in healthy livers and a robust induction of nuclear NFATc1 expression in liver biopsies of patients with progressive disease, characterised by macrovesicular steatosis and pronounced lobular inflammation (figure 1A,B). Consistent with a role of NFATc1 in disease acceleration, we observed a significant correlation of intrahepatic NFATc1 expression with NAFLD progression, determined by the NAS, the degree of fibrosis and the levels of liver enzymes in blood samples from patients with NASH (figure 1C–F). Prompted by these findings, we expanded our analysis on NFATc1 activation in NAFLD progression and studied NFATc1 induction and nuclear localisation in a mouse model of progressive NAFLD. For this purpose, we fed mice with a high-fat western diet (WD) for 20 weeks (figure 2A). This model is an excellent tool for studying the incremental steps of NAFLD progression.[33] In line with previous reports, WD treated mice developed hepatic steatosis with ballooned hepatocytes and a mild-to-moderate form of lobular inflammation with significant

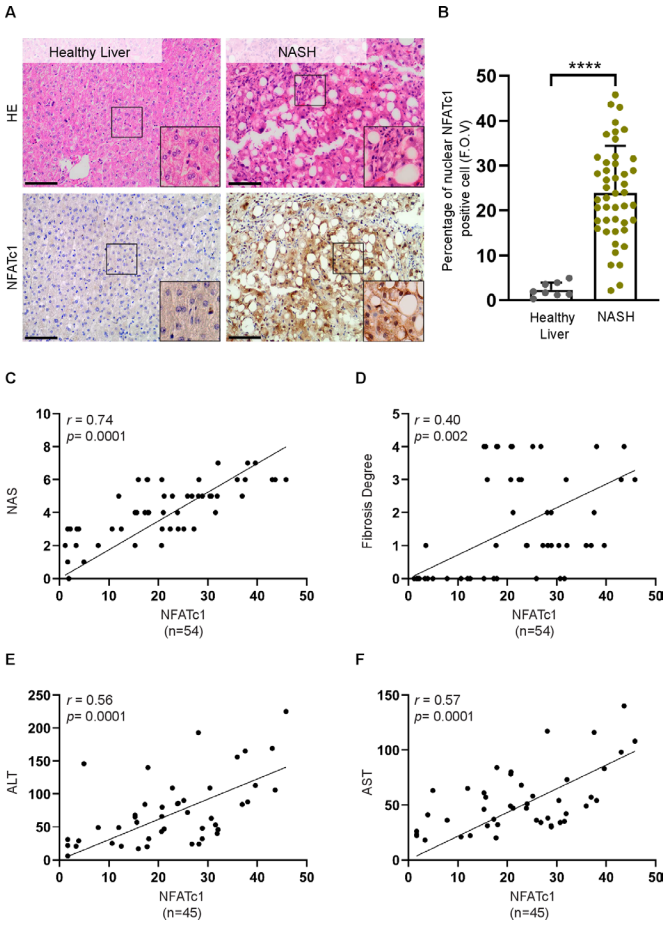

Figure 1 Hepatocyte-specific NFATc1 activation in progressive non-alcoholic liver disease (NAFLD). (A) Sections of healthy human liver (n=8) and non-alcoholic steatohepatitis (NASH) (n=46) were analysed by H&E staining and immunohistochemistry for NFATc1. Representative images are shown, scale bar=50 µm. (B) Percentage of nuclear NFATc1-positive hepatocytes per field of view in samples from healthy liver and NASH. Statistical analysis was performed by unpaired t-test. Data are shown as mean±SD, ****p≤0.0001. Simple linear regression analysis revealed a significant correlation of hepatic NFATc1 expression levels with (A) NAS (NAFLD activity score), (B) the degree of fibrosis, (C) ALT levels and (D) AST levels.

recruitment of CD45-positive immune cells and marked fibrosis (figure 2B–D). Moreover, and consistent with our findings in progressive human NAFLD, immunohistochemistry and western blot analysis confirmed a strong induction and nuclear accumulation of NFATc1 in hepatocytes of NASH livers (figure 2E,F). Taken together, these studies performed in progressive human and murine NAFLD provided first experimental evidence for a role of NFATc1 activation in disease acceleration.

NFATc1 activation drives fatty acids-induced steatohepatitis (NASH) and fibrosis

To study whether nuclear NFATc1 activation is indeed causally involved in the initiation and progression of NAFLD, we generated genetically modified mice with either hepatocyte-specific nuclear activation (*Alb-Cre; NFATc1$^{c.a}$*. (*NFATc1$^{c.a}$*.)) or depletion (*Alb-Cre; NFATc1$^{\Delta/\Delta}$* (*NFATc1$^{\Delta/\Delta}$*)) of NFATc1. Animals with endogenous NFATc1 expression (*Alb-Cre*) were used as controls. Eight-weeks old mice of all genotypes were fed with control diet (CD) or WD for defined treatment periods up to 20 weeks (figure 3A). As expected, treatment of *Alb-Cre* control mice with WD resulted in (1) increased liver and body weight (online supplemental figure 1A–C), (2) progressive steatosis with accumulation of intrahepatic triglycerides (figure 3B, (online supplemental figure 1D) and (3) an increasing inflammatory response with recruitment of CD45-positive immune cells and pronounced collagen deposition (figure 3B–H). Importantly, however, a comparable increase in inflammation, CD45-positive cell recruitment and collagen deposition was observed (figure 3B–F) in transgenic mice with hepatocyte-specific activation of nuclear NFATc1 (*NFATc1$^{c.a}$*.), and this damage again increased on feeding with high-fat WD. Importantly and consistent with our observations in patients with NASH, we also measured elevated serum ALT levels in mice with NFATc1$^{c.a}$. driven NAFLD progression (online supplemental figure 1E). In contrast, disease progression was greatly reduced in mice with hepatocyte-specific NFATc1 deficiency (*NFATc1$^{\Delta/\Delta}$*) and hence, NFATc1 depletion reduced the extent of liver fibrosis and inflammation and almost completely abolished the recruitment of CD45-positive cells (figure 3B–F). Of note, we could not observe NFATc1 addiction in the development of hepatic steatosis, such that neither ectopic expression nor genetic deletion of the transcription factor had a significant effect on the extent of hepatic fat accumulation after WD (figure 3G,H, online supplemental figure 1D,F). Collectively, these findings substantiate a causal role of NFATc1 in the progression of NAFLD and show that activation of the transcription factor in liver cells, for example, as a consequence of high-fat diet, results in pronounced inflammation and fibrosis.

Lipotoxic fatty acids induce NFATc1 signaling activation in hepatocytes

Free fatty acids (FFAs) are main contributors to the intrahepatic triglyceride pool and recent studies suggest that lipotoxic FFAs play a particularly important role in the development and progression of NAFLD. This applies in particular to the saturated FFA palmitate, which has a pronounced cell-damaging effect on liver cells and is found in particularly high concentrations in the blood of patients with NASH.[34] To directly test whether exposure to palmitate induces NFATc1 expression in liver cells, we treated primary hepatocytes and AML12 cells with increasing concentrations of the highly lipotoxic fatty acid (online supplemental figure 2A and figure 4A–G). In fact, treatment with palmitate led to a remarkable and dose-dependent increase of NFATc1 expression in both cell models and on mRNA and protein levels as well (online supplemental figure 2A and figure 4A–D). By contrast, incubation with oleate, a non-lipotoxic FFA failed to induce NFATc1 expression in primary hepatocytes even at high doses and despite significant accumulation of liver cell steatosis, as evidenced by Oil-Red-O staining (online supplemental figure 2A,B). Palmitate and oleate are among the most abundant FFAs, accounting for more than half of total plasma FFAs, and it has been shown that the cell toxic effects of palmitate can be counteracted by coexposure to oleate. In line with this, coadministration of non-lipotoxic oleate in liver cells inhibited NFATc1 induction by palmitate, supporting the idea that induction of the Ca^{2+}-regulated transcription factor in NAFLD progression is primarily a consequence of FFA-induced lipotoxicity—rather than fat accumulation per se. A close connection between lipotoxicity-induced cell stress and impaired Ca^{2+} signalling homeostasis has already been demonstrated in liver cells. Here, we extend these findings and show that exposure to palmitate initiates a dose-dependent shift of

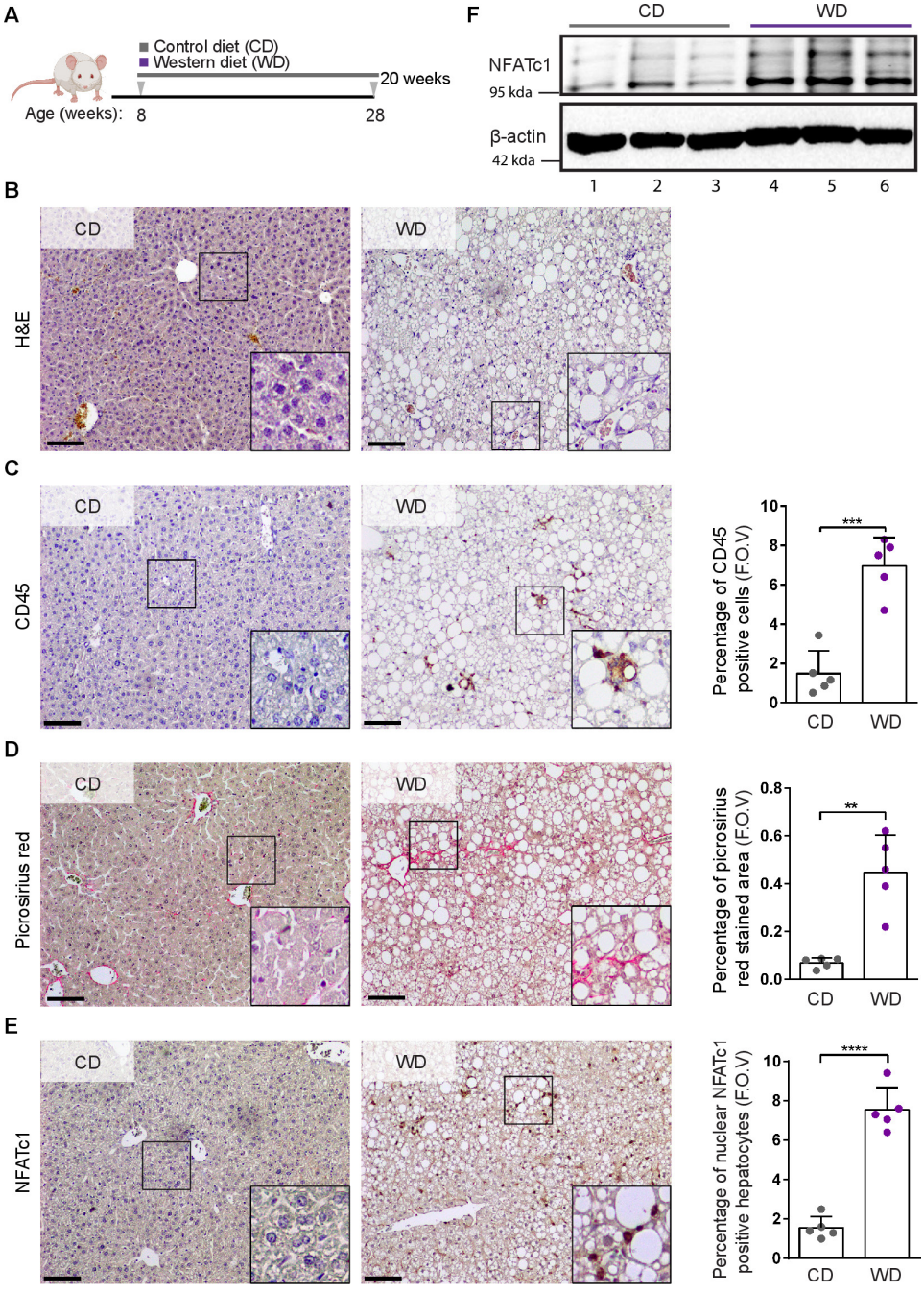

Figure 2 NFATc1 induction and non-alcoholic fatty liver disease (NAFLD) progression in western diet (WD) fed mice. (A) Schematic representation of the diet feeding protocol. Eight weeks old C57BL/6 wild-type mice were treated with either control diet (CD) or WD for 20 weeks. (B) Mice were sacrificed, and liver sections were analysed by H&E staining and immunohistochemical analysis for (C) CD45, (D) picrosirius red and (E) NFATc1 expression. Representative results are shown. Scale bars=100 µm. Quantification analyses were performed, and results were illustrated as percentage of CD45-positive cells, percentage of picrosirius red stained area and the percentage of nuclear NFATc1-positive hepatocytes in livers sections obtained from CD-treated and WD-treated mice (n=5). Statistical analysis was performed by unpaired t-test. Data are shown in mean±SD, **p<0.005, ***p<0.0005, ****p<0.0001. (F) Representative western blot of NFATc1 expression in liver tissue lysates of 20 weeks old mice treated with either CD (n=3, lane 1–3) or WD (n=3, lane 4–6). Each lane represents liver lysates from individual mice. WD-treated mice express high levels of active NFATc1, indicated by strong increase of the lower band.

Ca^{2+} from ER stores to the cytosol of fatty liver cells (online supplemental figure 2C–E). A rise in cytosolic Ca^{2+} causes activation of various cell-type dependent stress response pathways,[35] most notably the NFATc1 signalling and transcription factor. In fact, palmitate-induced accumulation of cytosolic Ca^{2+} is paralleled by robust NFATc1 activation in hepatocytes, evidenced by a particularly strong increase of the lower band that reflects the hypophosphorylated active status of the transcription factor (figure 4C,D, online supplemental figure 2A). Accordingly, reporter gene assays and immunofluorescence staining confirmed nuclear accumulation and increased transcriptional activity of NFATc1 in response to palmitate treatment in both cell lines (figure 4E–G; online supplemental figure 2F).

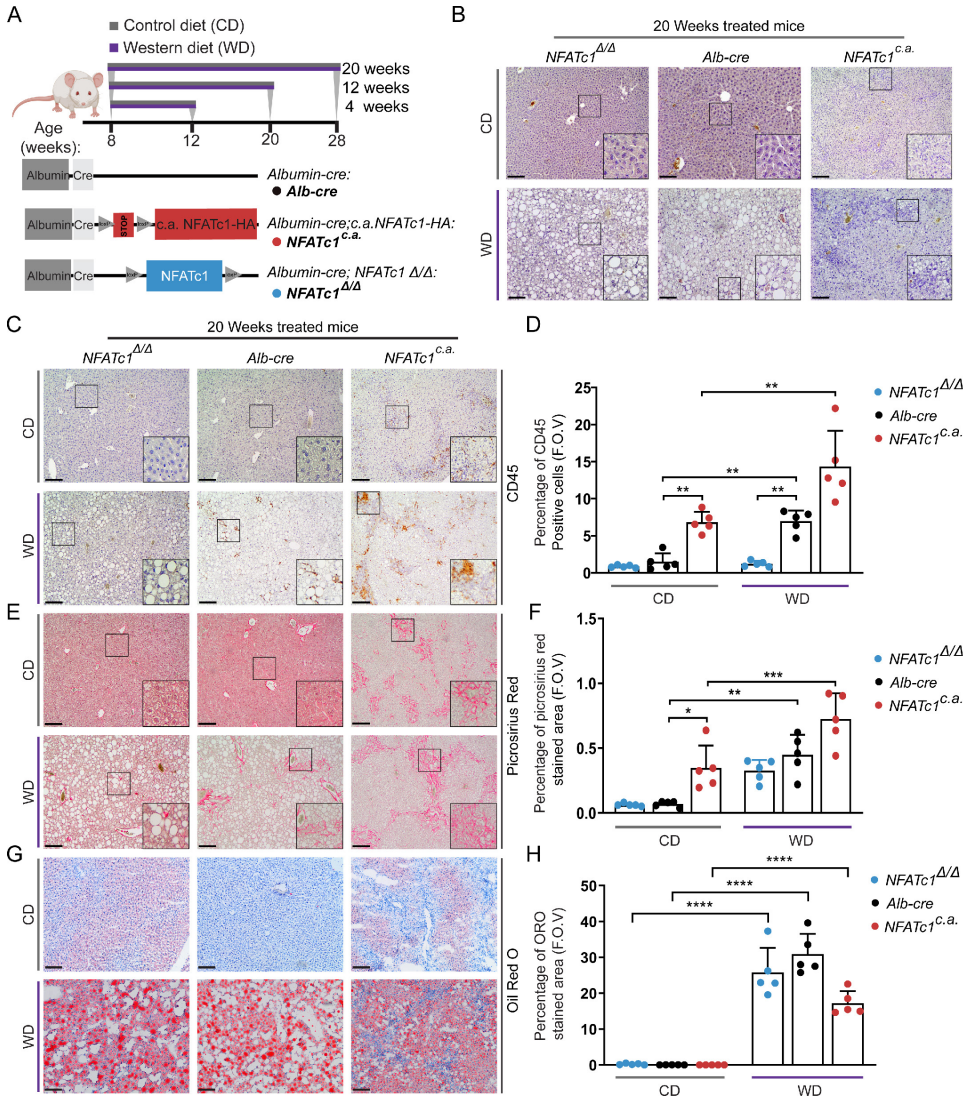

Figure 3 NFATc1 activation in hepatocytes drives liver inflammation and fibrosis. (A) Schematic depiction of genetically modified mice with hepatocyte-specific NFATc1 expression (*Alb-Cre; NFATc1$^{c.a}$*. (*NFATc1$^{c.a}$*.) or deletion Alb-Cre; *NFATc1$^{Δ/Δ}$* (*NFATc1$^{Δ/Δ}$*)) along with the feeding schedule for 4, 12 and 20 weeks, respectively. (B) H&E analysis of liver sections from CD (left) and WD (right) treated mice are shown (n=5). Scale bar=100 µm. Representative images of immunohistochemical analysis and quantification for (C–D) CD45, (E–F) picrosirius red staining and (G–H) oil-red-o staining in the livers of 20-week CD-treated and WD-treated *NFATc1$^{Δ/Δ}$*, *Alb-Cre* and *NFATc1$^{c.a}$*. mice (n=5). Statistical analysis was performed by two-way analysis of variance and data are shown as mean±SD where p values are *p<0.05, **p<0.005, ***p<0.0005.

NFATc1 promotes ER stress-induced UPR and immune signaling in liver

To explore the underlying mechanisms by which NFATc1 regulates NAFLD progression, we next studied NFATc1-dependent gene expression and performed transcriptome analysis in AML12 cells. For this purpose, we extracted mRNA from (HA-tagged) c.n.NFATc1 or control plasmid transfected AML12 cells and carried out RNA-Seq analysis. For transfection control, we performed western blot and qRT-PCR analysis (figure 5A). PCA demonstrated distinct clustering of NFATc1-induced and control profiles (online supplemental figure 3A). RNA-Seq analysis revealed 636 differentially expressed genes, of which 471 genes were upregulated following nuclear activation of NFATc1 (figure 5B). Moreover, reactome pathway analysis further demonstrated that the most significantly enriched pathways are involved in either interferon and cytokine/chemokine signalling, cell death regulation or cell stress responses (figure 5C). Specifically, NFATc1 activation led to a highly significant and reproducible induction of proinflammatory cytokines (eg, *Ccrl2 and Ccl5*) and chemokines (eg, *Cxcl2, Cxcl9 Cxcl10, Cxcl11)*, inflammatory transcription factors (eg, *Stat1* and *Stat2*) and cell death marker genes (eg, *Bak1*, *Casp7 and Tnfsf10*) (figure 5D). Noteworthy, we confirmed NFATc1-dependent regulation of the identified inflammatory cytokines and chemokines, for example, *IL-1β, Ccl5*, *Cxcl9*, *Cxcl10* and *Cxcl11* in the murine NAFLD progression model (online supplemental figure 3B,C).

Most importantly, our transcriptome analysis also uncovered a strong and highly reproducible link between NFATc1 activation and induction of ER stress pathways, particularly the terminal PERK (protein-kinase RNA-like ER kinase) UPR. In fact, we found a significant (20-fold) induction of various signalling components, for example, *Eif2ak2*, *Atf3 and Ddit3 (Chop)* on NFATc1 activation (figure 5C,D). The UPR can be induced by activation of the three canonical ER-resident stress sensor proteins ATF6, IRE1 and PERK following perturbation of protein homeostasis in the ER lumen. On activation, UPR

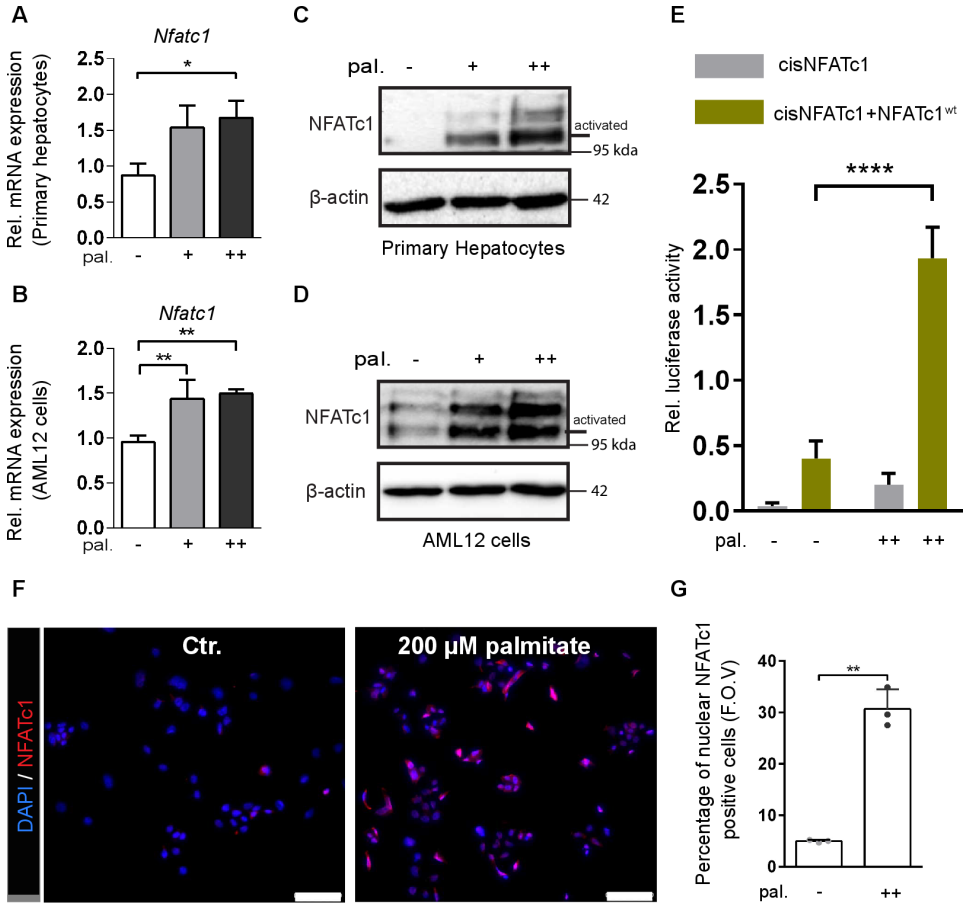

Figure 4 Lipotoxic fatty acids cause NFATc1 activation. (A–B) Expression of NFATc1 mRNA in (A) primary mouse hepatocytes and (B) AML12 cells following treatment with 100 µM (+) and 200 µM (++) palmitate (pal.) for 12 hours. NFATc1 gene expression was analysed by qRT-PCR and is shown as 'relative mRNA levels' compared with untreated control. (C–D) Induction of NFATc1 protein expression in (C) primary mouse hepatocytes and (D) AML12 cells treated with 100 µM (+) and 200 µM (++) palmitate (pal.) for 12 hours. The lower band represents the active state of NFATc1. (E) Dual luciferase reporter gene assay was performed in hepatocytes from *Alb-cre* mice to verify palmitate induced transcriptional activation of NFATc1. Cells were cotransfected with an NFAT responsive promoter luciferase reporter construct in combination with either an empty vector or NFATc1 wild-type (NFATc1^{wt}) expression vector, and subsequently treated with 200 µM palmitate (pal.) for 24 hours. (F) NFATc1 immunofluorescence in AML12 cells demonstrating nuclear translocation of the transcription factor following treatment with 200 µM palmitate for 12 hours. Scale bar=100 µm. (G) Quantitative analysis of palmitate-induced nuclear NFATc1 localisation in AML12 cells. Statistical analysis was performed by one-way analysis of variance (ANOVA) (A,B), two-way ANOVA (E) and by unpaired t-test (G). Data are shown as mean±SD, *p≤0.05, **p≤0.005 and ****p≤0.0001.

signalling controls multiple cell mechanisms to reduce protein synthesis and increase the protein folding capacity. However, while physiological UPR signalling allows cells to maintain cellular homeostasis, excessive UPR activation can lead to pathological changes, such as cell damage and death. It has been shown, for instance, that chronic ER stress sensing and UPR signalling can result from lipotoxic cell damage (eg, palmitate) and subsequently triggers cell death and inflammation in NAFLD progression.[36–38] This is particularly true for PERK kinase-driven signalling through the Eif2α-ATF4-CHOP pathway.[36 38 39] High levels of PERK and CHOP, for instance, are found in patients with NASH and specifically in those patients with a deleterious course of the disease.[40] Here, we show that NFATc1 activation indeed induces PERK kinase signalling but also phosphorylation of PKR, another member of the eif2α kinase family, involved in cellular stress responses and UPR signalling (figure 6). In detail, NFATc1 activation—either genetically or following stimulation by palmitate—caused increased PERK (pPERK), PKR (pPKR) and Eif2α (pEif2α) phosphorylation and subsequent induction of the core downstream signalling components, for example, CHOP, both in cultured AML12 cells and primary hepatocytes (online supplemental figure 4A, figure 6A–E). Similar results were found in WD-treated mice (figure 6F).

Moreover, terminal UPR responses were strongly impaired following NFATc1 silencing (figure 6A–E, (online supplemental figure 4B–D) in vitro and in the murine NAFLD progression model, even on prolonged exposure to WD (figure 6F). Of note, NFATc1 activation appears not to be relevant for the activation of the other two ER stress sensors (IRE1/XBP1 and ATF6) in liver cells and accordingly we could not observe NFATc1-dependent expression differences (online supplemental figure 4E,F) on palmitate treatment. This observation is also in line with previous reports demonstrating that although IRE1/XBP1 and ATF6 pathways can also up-regulate CHOP, the PERK pathway predominates in NAFLD progression through selective upregulation of ATF4 translation, which subsequently induces transcription of CHOP to promote cell death.[3 41]

Together, these studies provide compelling evidence for a mechanistic link between lipotoxic fatty acids-induced NFATc1 activation in liver cells and the induction of the deleterious PERK/PKR-CHOP UPR pathway in progressive NAFLD.

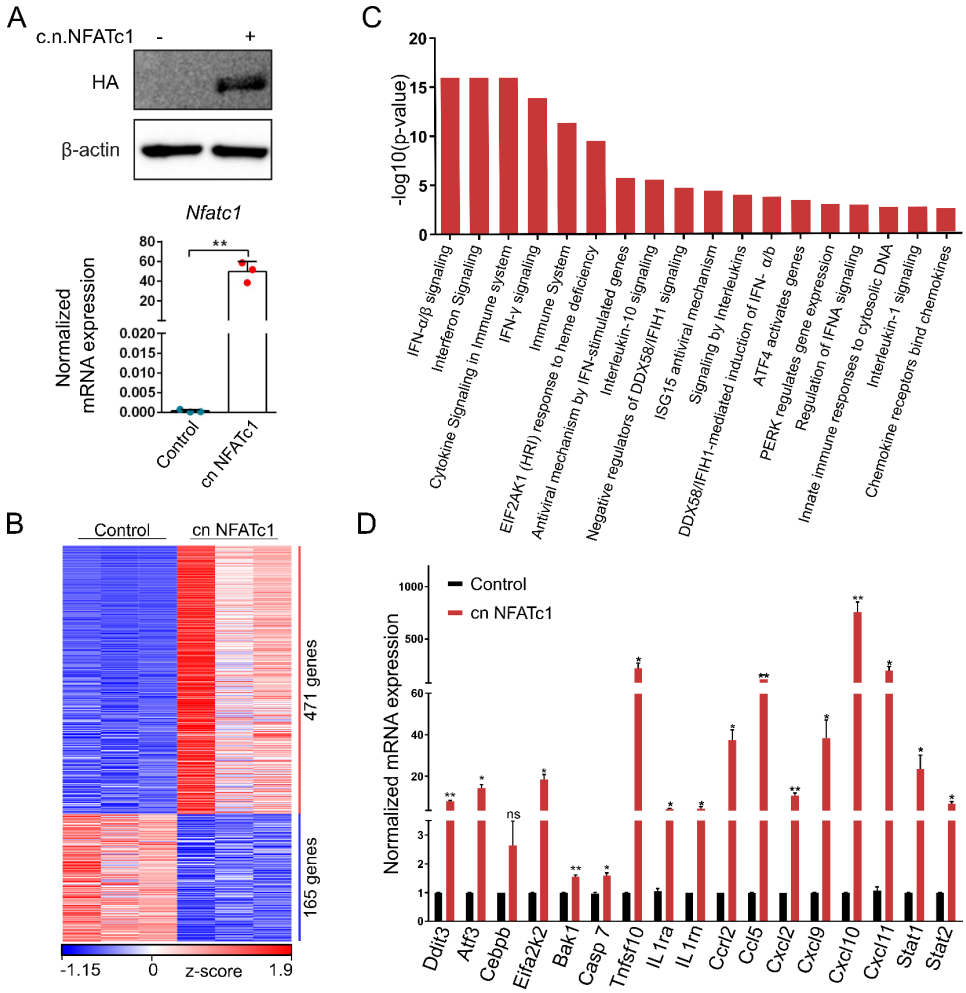

Figure 5 NFATc1 regulated gene signatures and signalling mechanisms. (A) Representative western blot and qRT-PCR showing successful NFATc1 transfection and expression in AML12 cells. (B) Heatmap depicting z-scores of significantly differentially expressed genes in RNA-Seq analysis on NFATc1 overexpression in AML12 cells. (C) Reactome pathway classification analysis demonstrating the most significantly regulated NFATc1 gene signatures in AML12 cells identified by RNA-Seq (log2fold values≥0.5/≤−0.5; p≤0.05; base mean>10). (D) qRT-PCR validation of differentially regulated candidate genes on NFATc1 activation in AML12 cells. Data are shown in mean±SD, p values are *p<0.05, **p<0.005. Statistical analysis was performed by unpaired t-test.

NFATc1 depletion protects liver cells from ER-stress-induced inflammasome activation and apoptosis

Recent studies have unequivocally shown that chronic ER stress uses the PERK-CHOP signalling pathway to promote apoptosis and activation of the NOD-like receptor family pyrin domain containing 3 (NLRP3) inflammasome.[37] NLRP3 is a multimeric protein complex that stimulates caspase-1 dependent cleavage of pro-interleukin-1β (pro-IL-1β) and gasdermin-D for induction of inflammation and a proinflammatory form of cell death, termed pyroptosis. Here, we examined whether terminal PERK-CHOP signalling activation promotes hepatocyte death and activation of NLRP3 driven pyroptosis in progressive NAFLD and if so, whether this is NFATc1 dependent. To this end, we analysed ER stress-induced NLRP3 inflammasome activation as well as caspase-1 mediated IL-1β and gasdermin cleavage in primary hepatocytes, AML-12 cells and transgenic mice livers with differential NFATc1 expression. Together, western blot, immunofluorescence and immunohistochemical analysis confirmed that lipotoxicity-induced UPR signalling promotes apoptosis (indicated by cleaved caspase-3) as well as NLRP3 inflammasome-induced cytokine release (indicated by cleaved IL-1β) and pyroptosis, as indicated by cleaved caspase-1 and increased gasdermin-D activation (C.GSDMD)) (figure 7A–F, online supplemental figure 4G,H). Importantly, UPR-driven inflammasome activation and cell death initiation require the presence of NFATc1 and therefore, genetic depletion of the transcription factor prevented palmitate-induced caspase-3 activation and blocked NLRP3-driven pyroptosis and IL-1β cleavage both in vitro and in the NAFLD progression model (figure 7A–F, online supplemental figure 4G,H). By contrast, and in line with our findings illustrated in online supplemental figure 2, non-lipotoxic oleate treatment neither induces NFATc1 activation nor terminal UPR signalling and subsequent NRLP3-inflammasome-induced cell death in primary hepatocytes (online supplemental figure 5).

Collectively, these experiments performed in primary hepatocytes and transgenic mice emphasise a key role of nuclear NFATc1 in driving terminal ER stress responses to foster NAFLD progression.

Inhibition of chronic ER stress responses attenuates NFATc1-induced NAFLD progression

Based on these results, we tested whether pharmacological inhibition of ER stress can impede NFATc1-triggered disease progression in NAFLD. To this end, we analysed the impact of tauroursodeoxycholic acid (TUDCA), a well-established inhibitor of ER stress responses on NFATc1-dependent mechanisms

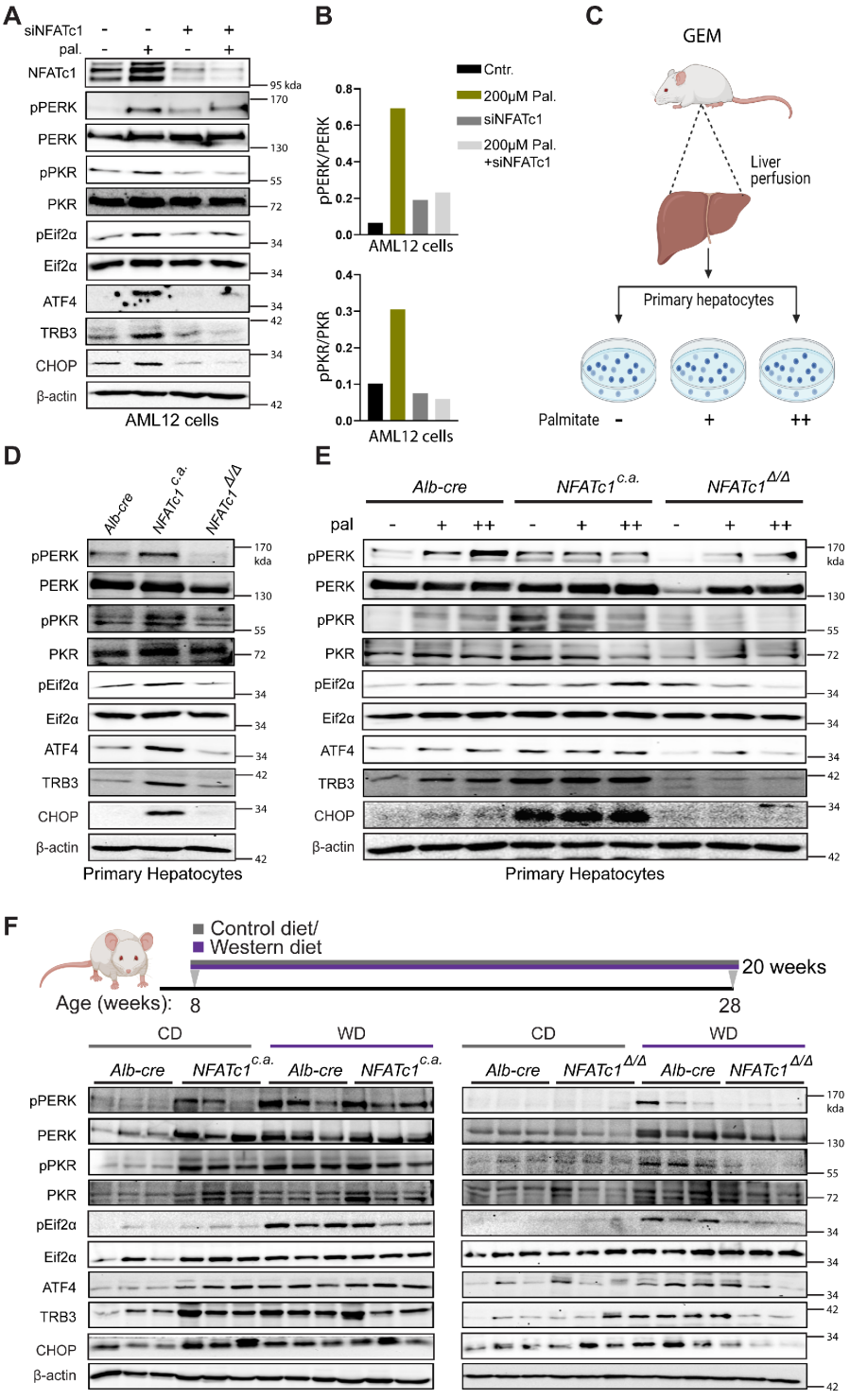

Figure 6 Nuclear NFATc1 promotes terminal unfolded protein response (UPR) signalling. (A) Immunoblot examination showing protein levels of NFATc1, pPERK, PERK, pPKR, PKR, ATF4, TRB3, p-Eif2α, Eif2α and CHOP in AML12 cells following 12 hours of palmitate (+=200 µM) exposure either alone or in combination with knock-down for NFATc1 (siNFATc1). (B) Densitometry graphs for pPERK/PERK and pPKR/PKR in AML12 cells treated with palmitate (200 µM) alone or in combination with siNFATc1. (C) Schematic illustration of primary hepatocytes isolation from transgenic mice with differential NFATc1 expression and subsequent palmitate treatment. (D) Representative western blot showing NFATc1-dependent protein levels of pPERK, PERK, pPKR, PKR, ATF4, TRB3, p-Eif2α, Eif2α and CHOP in primary hepatocytes. (E) Primary mouse hepatocytes were exposed to palmitate (+=100 µM and ++=200 µM) for 12 hours and alterations in pPERK, PERK, pPKR, PKR, ATF4, TRB3, p-Eif2α, Eif2α and CHOP levels were analysed by immunoblot. (F) Western blot analysis were conducted using liver tissue lysates from CD-treated and WD-treated genetically modified mice (GEM) models to determine fat-induced and NFATc1-dependent expression of pPERK, PERK, pPKR, PKR, ATF4, TRB3,p-Eif2α, Eif2α and CHOP.

and cell functions, both in primary hepatocytes and AML12 cells and in WD fed transgenic mice as well (figure 8, online supplemental figure 6A–C).

Consistent with results presented in figures 6 and 7, ER stress induction by either palmitate treatment or following c.n.NFATc1 transfection resulted in terminal UPR signalling (eg, CHOP)

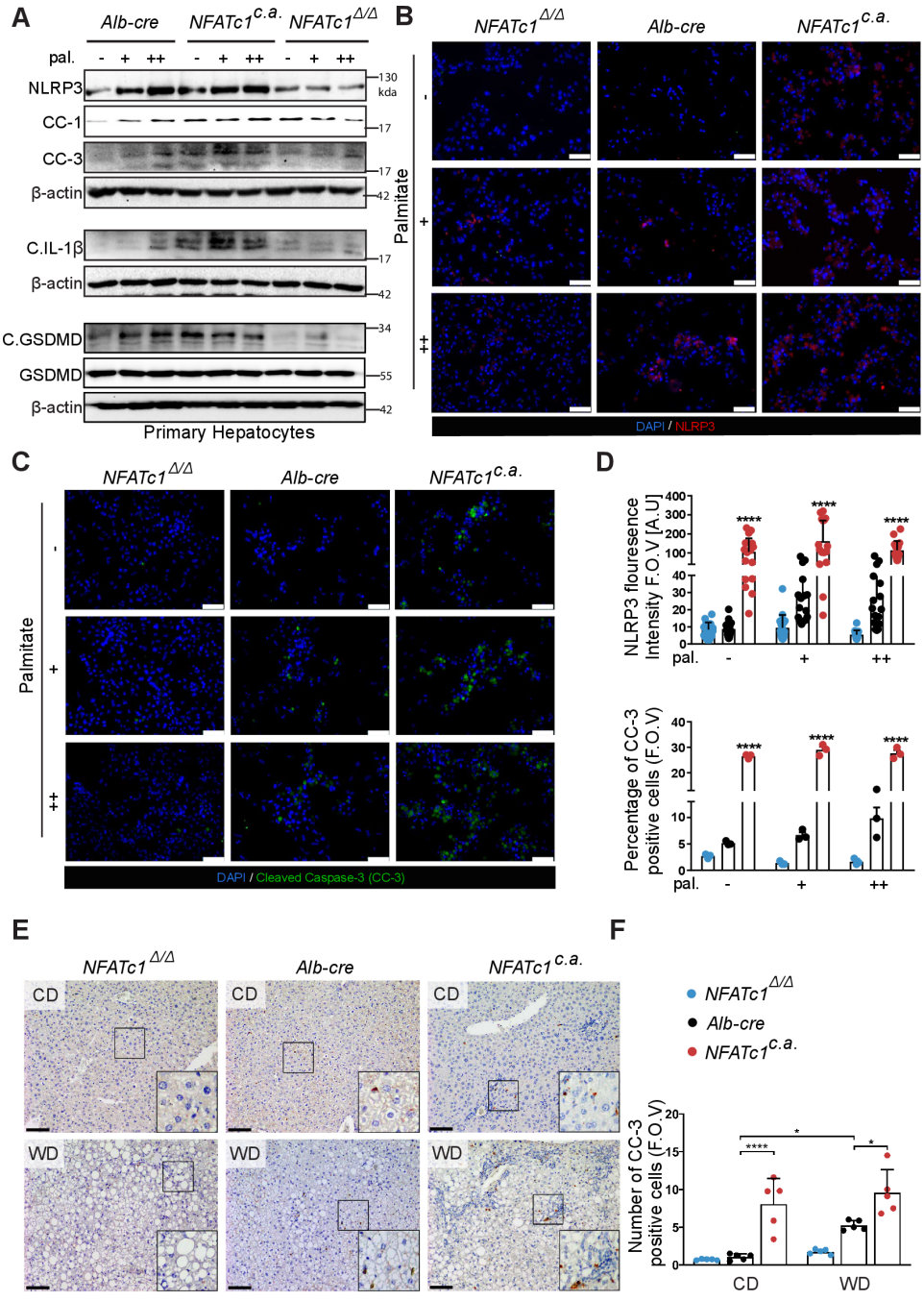

Figure 7 NFATc1-dependent cell death and inflammasome activation in vitro and in vivo. (A) Representative immunoblot displaying NFATc1-dependent changes in NLRP3, cleaved caspase-1 (CC-1), cleaved caspase 3 (CC-3), cleaved interleukin (IL)-1β, C.GSDMD and GSDMD (Gasdermin D) in primary hepatocytes following 12 hours of palmitate treatment (+=100 µM and ++=200 µM). (B) Immunofluorescence analysis of NLRP3 and (C) CC-3 in primary mouse hepatocytes after palmitate treatment. Scale bar=100 µm. (D) Graphs represent fluorescence intensity of NLRP3 and percentage of CC-3 positive hepatocytes (F.O.V). (E) Immunohistochemical analysis of CC-3 staining in liver sections of 20-week-treated mice. Scale bar=100 µm. (F) Quantitative analysis of CC-3 positive hepatocytes (F.O.V). Data are shown in mean±SD; p-values are *p<0.05, ****p<0.0001. Statistical analysis was performed using one-way analysis of variance (ANOVA) (D) and two-way ANOVA (F). CD, control diet; WD, western diet.

activation and subsequent induction of the NRLP3 inflammasome effector pathway both in vitro and in vivo. Intriguingly, however, application of TUDCA sufficiently blocked ER stress-induced terminal UPR signalling responses and inflammasome activation. In detail, we observed a significant blockade of terminal UPR (indicated by loss of CHOP expression), inhibition of cell death induction (reflected by cleaved-caspase-3) and inactivation of NRLP3-inflammasome mediated cytokine release (eg, IL-1β), even in the presence of active NFATc1 (figure 8A,B, online supplemental figure 6A). Similar effects were confirmed in the NAFLD progression model, in which TUDCA-mediated inhibition of terminal UPR signalling and subsequent NLRP3 activation was associated with a tremendous reduction of inflammation, recruitment of CD45-positive immune cells and hepatic fibrosis despite expression of constitutive active NFATc1 (figure 8D–I, online supplemental figure 6D–E).

Together, this study strongly supports an important role of NFATc1 in NAFLD progression and demonstrates that this

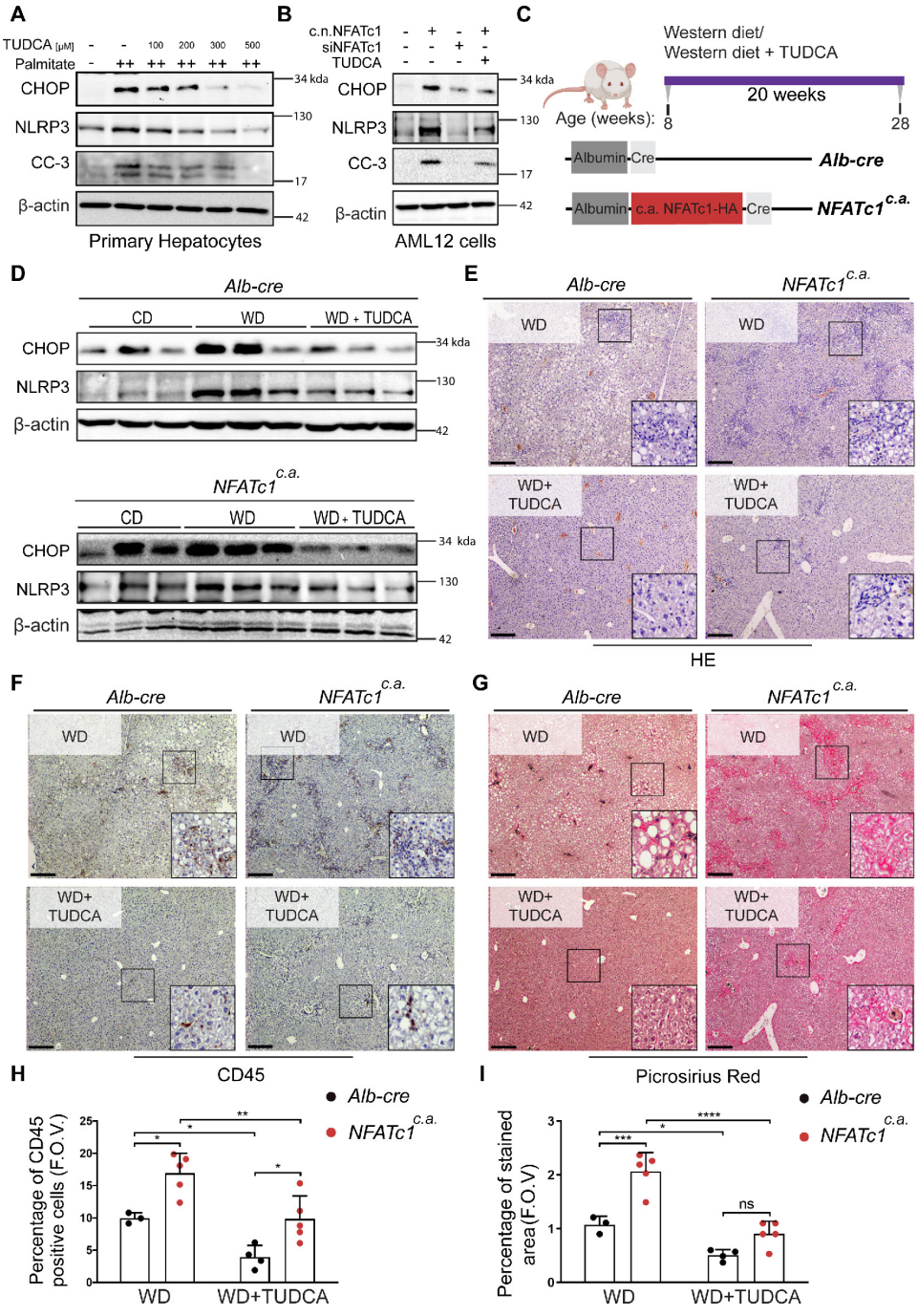

Figure 8 Tauroursodeoxycholic acid (TUDCA) attenuates NFATc1-dependent unfolded protein response (UPR) signalling-induced inflammation and fibrosis in progressive non-alcoholic liver disease (NAFLD). (A) Immunoblot shows protein expression of CHOP, NLRP3 and CC-3 in *Alb-cre* primary hepatocytes treated with palmitate (++=200 µM) alone or in combination with increasing concentrations of TUDCA (100–500 µM) in comparison to control-treated cells. (B) Protein levels of CHOP, NLRP3 and CC-3 were assessed in AML12 cells with constitutive activation of NFATc1 and in the presence or absence of 500 µM TUDCA for 12 hours. Cells transfected with siNFATc1 were used as control. (C) Schematic representation of the preventive treatment scheme. (D) Immunoblot showing protein levels of CHOP and NLRP3 in liver tissue lysates of 20 weeks treated *Alb-cre* mice and *NFATc1*$^{c.a.}$ mice. (E) H&E staining and immunohistochemical analysis for (F) CD45 and (G) picrosirius red staining. Scale bar=100 µm. (H) Graph represents percentage of CD45 positive cells and (I) percentage of picrosirius red stained area (F.O.V). Data are shown in mean±SD, p values are *p<0.05, **p<0.005, ***p<0.0005, ****p<0.0001. Statistical analysis was performed by two-way analysis of variance.

function is based on the regulation of chronic ER stress responses and subsequent NLRP3 inflammasome activation. Moreover, we provide evidence that pharmacological inhibition of ER stress responses (eg, via TUDCA) can overcome NFATc1-driven progression of the disease.

DISCUSSION

This study was designed to decipher key molecular mechanisms of NAFLD progression and hence to provide a rational basis for the development of new treatment strategies. We thereby focused on the calcium-responsive NFAT transcription factor family,

which controls a plethora of cellular processes in inflammation-associated and metabolic disorders, for example, insulin resistance and diabetes, obesity and cancer.[12 14 17 18 20] Here, we uncover an essential role of NFATc1 in the progression of NAFLD to NASH. Accordingly, NFATc1 expression and nuclear localisation are weak to absent in healthy livers but strongly induced in progressive NASH. Moreover, treatment with fatty acids, for example, palmitate or WD induces expression, nuclear translocation and transcriptional activity of NFATc1 both in primary and established hepatocytes as well as in mouse liver tissues. Furthermore, hepatocyte-specific activation of nuclear NFATc1 in mice livers—either following WD feeding or through genetic induction of the transcription factor (NFATc1$^{c.a}$)—fosters rapid acceleration of liver damage, as evidenced by increased tissue inflammation with recruitment of CD45-positive cells and progressive formation of hepatic fibrosis. These results, together with the observation that hepatocyte-specific genetic depletion of NFATc1 prevents fatty acids-induced NAFLD progression beyond the stage of hepatic steatosis, provided strong experimental evidence for a critical role of the Ca^{2+} responsive transcription factor in progressive NAFLD.

Mechanistically, NFATc1 promotes NAFLD acceleration through unrestricted ER stress signalling responses in liver cells. The ER is responsible for proper protein folding,[3 42] and it has been shown that defects in the calcium homeostasis or the ER protein folding machinery can cause ER stress and subsequent activation of the UPR pathway. The UPR pathway orchestrates a multitude of key regulatory mechanisms to repair ER stress including inhibition of protein synthesis and acceleration of ER protein degradation. In general, UPR activation is highly sufficient to repair transient and mild forms of ER stress.[3 37 43–46] However, if ER stress is severe and unresolved, it can cause persistent activation of the UPR signalling pathway and eventually leads to cell death, inflammasome activation and accelerated organ damage. Recent studies demonstrated that fat accumulation can trigger chronic ER stress and subsequent activation of the terminal UPR signalling cascade in hepatocytes.[3 7 11 37 47 48] Here, we show for the first time a fundamental role of the Ca^{2+} responsive transcription factor NFATc1 in ER stress-induced NAFLD progression. In detail, prolonged exposure to fatty acids induces expression, nuclear localisation and activity of NFATc1 in hepatocytes both in vitro and in mice with progressive NAFLD. Mechanistically, NFATc1 promotes ER stress sensing through terminal PERK-CHOP signalling and subsequently induces activation of NLRP3,[49–51] a macromolecular inflammasome complex involved in cell death initiation and inflammation.[7 36 38 48] The prominent function of the terminal PERK-CHOP pathway in chronic ER stress-driven NLRP3 inflammasome activation and apoptosis has been demonstrated in various disorders and especially in diseases related to metabolic disturbances.[47 48 52 53] In NAFLD, for instance, CHOP activation induces the NRLP3 inflammasome complex to promote hepatocyte death and inflammation in response to unresolved ER stress.[3 7 36] Our results not only confirm these previous observations, but in addition, demonstrate that NFATc1 activation is mandatory for fat-induced ER stress signalling through the PERK-CHOP branch and subsequent activation of the NRLP3 inflammasome pathway. Accordingly, genetic depletion of NFATc1 prevents liver cells from terminal UPR signalling, NRLP3 activation and cell death initiation both in primary hepatocytes and in liver tissues, even on longtime stimulation with high-fat diet.

Lastly, we assessed whether inhibition of chronic ER stress signalling can protect fatty livers from NFATc1-induced disease progression. For this purpose, we combined prolonged high-fat stimulation with application of TUDCA, a naturally occurring hydrophilic bile acid and taurine conjugate of ursodeoxycholic acid (UDCA), which is approved by Food and Drug Administration for the treatment of primary biliary cholangitis (PBC). Recent multicentre randomised clinical trials have shown that TUDCA presents the same level of safety and tolerability as UDCA for the treatment of PBC and may be even better to relieve symptoms of the disease, suggesting higher effectiveness of taurine conjugate in treatment of PBC.[54] The efficacy of TUDCA in cholestatic diseases was primarily attributed to its choleretic and cytoprotective effects on hepatocytes by increasing bile flow and biliary acid secretion.[55] Importantly, numerous preclinical studies have also demonstrated a remarkable therapeutic potential of TUDCA in non-cholestatic liver diseases and particularly in NAFLD, where it exerts strong cytoprotective effects through its ability to alleviate ER stress and to block terminal PERK-CHOP signalling.[7 36 56] Our results strongly support these efforts and provide a mechanistic rationale for the proposed efficacy of TUDCA in the prevention of NAFLD progression. We show that application of TUDCA effectively interferes with acceleration of the disease through inhibition of NFATc1-mediated ER stress sensing and terminal UPR signalling activation. Consistently, TUDCA treatment blocked NFATc1-induced CHOP-NRLP3 inflammasome activation and consequently reduced the degree of inflammation, apoptosis and fibrosis in the liver, even on long-term feeding with high-fat diet.

Taken together, this study identifies the calcium signalling responsive transcription factor NFATc1 as a key player in NAFLD progression. We show that NFATc1 drives fat-induced NASH through promotion of chronic ER stress responses and activation of the NRLP3 inflammasome. This study not only contributes to a better understanding of NFATc1 signalling in NAFLD but provides a mechanistic rationale for recent clinical trials aiming at pharmacological interference with chronic ER stress responses to prevent disease progression.

Author affiliations
[1]Department of Gastroenterology, Gastrointestinal Oncology and Endocrinology, University Medical Center Göttingen, Gottingen, Niedersachsen, Germany
[2]Gastrointestinal Unit, Massachusetts General Hospital, Harvard Medical School, Boston, Massachusetts, USA
[3]Molecular Physiology, Institute of Cardiovascular Physiology, University Medical Center Göttingen, Gottingen, Niedersachsen, Germany
[4]Institute for Microbiology and Hygiene, Medical Center-University of Freiburg, Freiburg, Baden-Württemberg, Germany
[5]Institute of Pharmacology and Toxicology, University Medical Center Göttingen, Gottingen, Niedersachsen, Germany
[6]Clinical Neuroscience, Max-Planck-Institute for Experimental Medicine, Goettingen, Niedersachsen, Germany
[7]Institute of Pathology, University Medical Center Göttingen, Gottingen, Germany

Twitter Shiv K Singh @ShivKSingh6

Acknowledgements We are very thankful to Higher education commission Pakistan, for providing doctorate scholarship to Muhammad Umair Latif. We are thankful to Dr. Nai-Ming Chen for his inputs in project development and Sarah L. Hanheide for her contributions in mouse breeding. We thank Gabriela Salinas from NGS Integrative Genomics Core Unit, Goettingen for sequencing of the samples. All the schematic illustrations were prepared using BioRender.com. Finally, we thank all the laboratory members for insightful discussions.

Contributors MUL performed most of the experiments, analysed and interpreted results. GES performed library preparation, RNA-seq analysis and figures designing. RR helped in the bioinformatics analysis for RNA-seq data. SM handled the mouse breeding and treatments. CSG and IS-T performed calcium measurement experiments in AML12 cells and AR performed in primary hepatocytes. KR facilitated in developing experimental plans and performed experiments. EH wrote all the approval applications for in-vivo experiments. SKS provided intellectual inputs and was involved in designing figures for the paper. AM facilitated in optimising primary hepatocyte isolation procedures. UJB provided support in IHC analysis and

manuscript proofreading. PS provided human tissues as well as helped in analysing the IHC staining. SCB and HB provided human NASH patient samples. AN provided scientific input in planning experiments and data interpretation. IB provided scientific inputs for this study and helped in planning experimental models. VE was the principal investigator of the study and was responsible for study concept and design. Together with MUL, he was also responsible for manuscript writing. VE is the guarantor and responsible for the overall content of the study.

Funding This project was primarily funded by the DFG (KFO-5002). Beside this it was supported by the German Cancer Aid to Shiv K. Singh (70112999; Max-Eder group), to Albrecht Neesse (70113213; Max-Eder group) and to Eisabeth Hessmann (70112108), the DFG grant to Shiv K. Singh and Elisabeth Hessmann (KFO-5002), the DFG grant to Ivan Bogeski (SFB1190 P17) and the Volkswagen-Stiftung/Ministry for Culture and Science in Lower Saxony (MWK) to Volker Ellenrieder (11-25 76251-12-3/16).

Competing interests None declared.

Patient consent for publication Not applicable.

Ethics approval All animal experiments were approved by local animal care and use committee (LAVES) and carried out according to the regulations of Federation of European Laboratory Animal Science Associations (FELASA).

Provenance and peer review Not commissioned; externally peer reviewed.

Data availability statement Data are available upon reasonable request. All data relevant to the study are included in the article or uploaded as supplementary information.

ORCID iDs
Christine Silvia Gibhardt http://orcid.org/0000-0001-5104-970X
Ioana Stejerean-Todoran http://orcid.org/0000-0002-4225-5912
Shiv K Singh http://orcid.org/0000-0002-5725-4058
Sebastian Christopher Bremer http://orcid.org/0000-0001-5481-0429
Albrecht Neesse http://orcid.org/0000-0002-3690-1957
Volker Ellenrieder http://orcid.org/0000-0001-9981-8571

REFERENCES

1 Wong RJ, Aguilar M, Cheung R, *et al*. Nonalcoholic steatohepatitis is the second leading etiology of liver disease among adults awaiting liver transplantation in the United States. *Gastroenterology* 2015;148:547–55.
2 Younossi ZM, Stepanova M, Afendy M, *et al*. Changes in the prevalence of the most common causes of chronic liver diseases in the United States from 1988 to 2008. *Clin Gastroenterol Hepatol* 2011;9:524–30. e1.
3 Lebeaupin C, Vallée D, Hazari Y, *et al*. Endoplasmic reticulum stress signalling and the pathogenesis of non-alcoholic fatty liver disease. *J Hepatol* 2018;69:927–47.
4 Byrne CD, Targher G. Nafld: a multisystem disease. *J Hepatol* 2015;62:S47–64.
5 Dowman JK, Tomlinson JW, Newsome PN. Pathogenesis of non-alcoholic fatty liver disease. *QJM* 2010;103:71–83.
6 Berlanga A, Guiu-Jurado E, Porras JA, *et al*. Molecular pathways in non-alcoholic fatty liver disease. *Clin Exp Gastroenterol* 2014;7:221.
7 Lebeaupin C, Proics E, de Bieville CHD, *et al*. Er stress induces NLRP3 inflammasome activation and hepatocyte death. *Cell Death Dis* 2015;6:e1879.
8 Csak T, Ganz M, Pespisa J, *et al*. Fatty acid and endotoxin activate inflammasomes in mouse hepatocytes that release danger signals to stimulate immune cells. *Hepatology* 2011;54:133–44.
9 Kim KH, Lee M-S. Pathogenesis of nonalcoholic steatohepatitis and hormone-based therapeutic approaches. *Front Endocrinol* 2018;9:485.
10 Petrasek J, Bala S, Csak T, *et al*. Il-1 receptor antagonist ameliorates inflammasome-dependent alcoholic steatohepatitis in mice. *J Clin Invest* 2012;122:3476–89.
11 Wree A, McGeough MD, Peña CA, *et al*. Nlrp3 inflammasome activation is required for fibrosis development in NAFLD. *J Mol Med* 2014;92:1069–82.
12 Pan M-G, Xiong Y, Chen F. Nfat gene family in inflammation and cancer. *Curr Mol Med* 2013;13:543–54.
13 Tripathi P, Wang Y, Coussens M, *et al*. Activation of NFAT signaling establishes a tumorigenic microenvironment through cell autonomous and non-cell autonomous mechanisms. *Oncogene* 2014;33:1840–9.
14 Heit JJ, Apelqvist AA, Gu X, *et al*. Calcineurin/Nfat signalling regulates pancreatic beta-cell growth and function. *Nature* 2006;443:345–9.
15 Mancini M, Toker A. Nfat proteins: emerging roles in cancer progression. *Nat Rev Cancer* 2009;9:810–20.
16 Daniel C, Gerlach K, Väth M, *et al*. Nuclear factor of activated T cells - a transcription factor family as critical regulator in lung and colon cancer. *Int J Cancer* 2014;134:1767–75.
17 Buchholz M, Schatz A, Wagner M, *et al*. Overexpression of c-myc in pancreatic cancer caused by ectopic activation of NFATc1 and the Ca2+/calcineurin signaling pathway. *Embo J* 2006;25:3714–24.
18 Chen N-M, Singh G, Koenig A, *et al*. Nfatc1 links EGFR signaling to induction of SOX9 transcription and Acinar-Ductal transdifferentiation in the pancreas. *Gastroenterology* 2015;148:1024–34. e9.
19 Baumgart S, Chen N-M, Siveke JT, *et al*. Inflammation-Induced NFATc1-STAT3 transcription complex promotes pancreatic cancer initiation by KrasG12D. *Cancer Discov* 2014;4:688–701.
20 Singh SK, Chen N-M, Hessmann E, *et al*. Antithetical NFATc1-Sox2 and p53-miR200 signaling networks govern pancreatic cancer cell plasticity. *Embo J* 2015;34:517–30.
21 Zhang X, Gibhardt CS, Will T, *et al*. Redox signals at the ER-mitochondria interface control melanoma progression. *Embo J* 2019;38:e100871.
22 Wang S, Kang X, Cao S, *et al*. Calcineurin/NFATc1 pathway contributes to cell proliferation in hepatocellular carcinoma. *Dig Dis Sci* 2012;57:3184–8.
23 Zhu R, Baker SS, Moylan CA, *et al*. Systematic transcriptome analysis reveals elevated expression of alcohol-metabolizing genes in NAFLD livers. *J Pathol* 2016;238:531–42.
24 Du M, Wang X, Yuan L, *et al*. Targeting NFATc4 attenuates non-alcoholic steatohepatitis in mice. *J Hepatol* 2020;73:1333–46.
25 Takahashi Y, Fukusato T. Histopathology of nonalcoholic fatty liver disease/ nonalcoholic steatohepatitis. *World Journal of Gastroenterology* 2014;20:15539.
26 Aliprantis AO, Ueki Y, Sulyanto R, *et al*. Nfatc1 in mice represses osteoprotegerin during osteoclastogenesis and dissociates systemic osteopenia from inflammation in cherubism. *J Clin Invest* 2008;118:3775–89.
27 Chen N-M, Neesse A, Dyck ML, *et al*. Context-Dependent epigenetic regulation of nuclear factor of activated T cells 1 in pancreatic plasticity. *Gastroenterology* 2017;152:1507–20. e15.
28 Gkretsi V, Apte U, Mars WM, *et al*. Liver-Specific ablation of integrin-linked kinase in mice results in abnormal histology, enhanced cell proliferation, and hepatomegaly. *Hepatology* 2008;48:1932–41.
29 Afgan E, Baker D, Batut B, *et al*. The Galaxy platform for accessible, reproducible and collaborative biomedical analyses: 2018 update. *Nucleic Acids Res* 2018;46:W537–44.
30 Kim D, Pertea G, Trapnell C, *et al*. TopHat2: accurate alignment of transcriptomes in the presence of insertions, deletions and gene fusions. *Genome Biol* 2013;14:R36–13.
31 Anders S, Pyl PT, Huber W. HTSeq--a Python framework to work with high-throughput sequencing data. *Bioinformatics* 2015;31:166–9.
32 Love MI, Huber W, Anders S. Moderated estimation of fold change and dispersion for RNA-Seq data with DESeq2. *Genome Biol* 2014;15:1–21.
33 Machado MV, Michelotti GA, Xie G, *et al*. Mouse models of diet-induced nonalcoholic steatohepatitis reproduce the heterogeneity of the human disease. *PLoS One* 2015;10:e0127991.
34 Ogawa Y, Imajo K, Honda Y, *et al*. Palmitate-Induced lipotoxicity is crucial for the pathogenesis of nonalcoholic fatty liver disease in cooperation with gut-derived endotoxin. *Sci Rep* 2018;8:1–14.
35 Oh-hora M, Rao A. The calcium/NFAT pathway: role in development and function of regulatory T cells. *Microbes Infect* 2009;11:612–9.
36 Nakagawa H, Umemura A, Taniguchi K, *et al*. Er stress cooperates with hypernutrition to trigger TNF-dependent spontaneous HCC development. *Cancer Cell* 2014;26:331–43.
37 Lebeaupin C, Vallee D, *et al*. Role of ER stress in inflammasome activation and non-alcoholic fatty liver disease progression. *Single Cell Biol* 2016;5:140.
38 Han CY, Rho HS, Kim A, *et al*. Fxr inhibits endoplasmic reticulum stress-induced NLRP3 inflammasome in hepatocytes and ameliorates liver injury. *Cell Rep* 2018;24:2985–99.
39 Liu X, Green RM. Endoplasmic reticulum stress and liver diseases. *Liver Res* 2019;3:55–64.
40 Toriguchi K, Hatano E, Tanabe K, *et al*. Attenuation of steatohepatitis, fibrosis, and carcinogenesis in mice fed a methionine-choline deficient diet by CCAAT/enhancer-binding protein homologous protein deficiency. *J Gastroenterol Hepatol* 2014;29:1109–18.
41 Malhi H, Kaufman RJ. Endoplasmic reticulum stress in liver disease. *J Hepatol* 2011;54:795–809.
42 Adams CJ, Kopp MC, Larburu N, *et al*. Structure and molecular mechanism of ER stress signaling by the unfolded protein response signal activator IRE1. *Front Mol Biosci* 2019;6:11.
43 Lin JH, Walter P, Yen TSB. Endoplasmic reticulum stress in disease pathogenesis. *Annu Rev Pathol* 2008;3:399–425.
44 Liu L, Zhao M, Jin X, *et al*. Adaptive endoplasmic reticulum stress signalling via IRE1α-XBP1 preserves self-renewal of haematopoietic and pre-leukaemic stem cells. *Nat Cell Biol* 2019;21:328–37.

45 Chan JY, Luzuriaga J, Maxwell EL, *et al*. The balance between adaptive and apoptotic unfolded protein responses regulates β-cell death under ER stress conditions through XBP1, CHOP and JNK. *Mol Cell Endocrinol* 2015;413:189–201.
46 Lake AD, Novak P, Hardwick RN, *et al*. The adaptive endoplasmic reticulum stress response to lipotoxicity in progressive human nonalcoholic fatty liver disease. *Toxicol Sci* 2014;137:26–35.
47 Maiers JL, Malhi H. Endoplasmic reticulum stress in metabolic liver diseases and hepatic fibrosis. *Semin Liver Dis* 2019;39:235–48.
48 Zhu Y, Guan Y, Loor JJ, *et al*. Fatty acid-induced endoplasmic reticulum stress promoted lipid accumulation in calf hepatocytes, and endoplasmic reticulum stress existed in the liver of severe fatty liver cows. *J Dairy Sci* 2019;102:7359–70.
49 Jiang S, Zhang E, Zhang R, *et al*. Altered activity patterns of transcription factors induced by endoplasmic reticulum stress. *BMC Biochem* 2016;17:8.
50 Son G-Y, Subedi KP, Ong HL, *et al*. STIM2 targets Orai1/STIM1 to the AKAP79 signaling complex and confers coupling of Ca^{2+} entry with NFAT1 activation. *Proc Natl Acad Sci U S A* 2020;117:16638–48.
51 Jang S-I, Ong HL, Liu X, *et al*. Up-Regulation of store-operated Ca2+ entry and nuclear factor of activated T cells promote the acinar phenotype of the primary human salivary gland cells. *J Biol Chem* 2016;291:8709–20.
52 Bronner DN, Abuaita BH, Chen X, *et al*. Endoplasmic reticulum stress activates the inflammasome via NLRP3- and Caspase-2-Driven mitochondrial damage. *Immunity* 2015;43:451–62.
53 Ji T, Han Y, Yang W, *et al*. Endoplasmic reticulum stress and NLRP3 inflammasome: crosstalk in cardiovascular and metabolic disorders. *J Cell Physiol* 2019;234:14773–82.
54 Ma H, Zeng M, Han Y, *et al*. A multicenter, randomized, double-blind trial comparing the efficacy and safety of TUDCA and UDCA in Chinese patients with primary biliary cholangitis. *Medicine* 2016;95:e5391.
55 Paumgartner G, Beuers U. Ursodeoxycholic acid in cholestatic liver disease: mechanisms of action and therapeutic use revisited. *Hepatology* 2002;36:525–31.
56 Uppala JK, Gani AR, Ramaiah KVA. Chemical chaperone, TUDCA unlike PBA, mitigates protein aggregation efficiently and resists ER and non-ER stress induced HepG2 cell death. *Sci Rep* 2017;7:1–13.

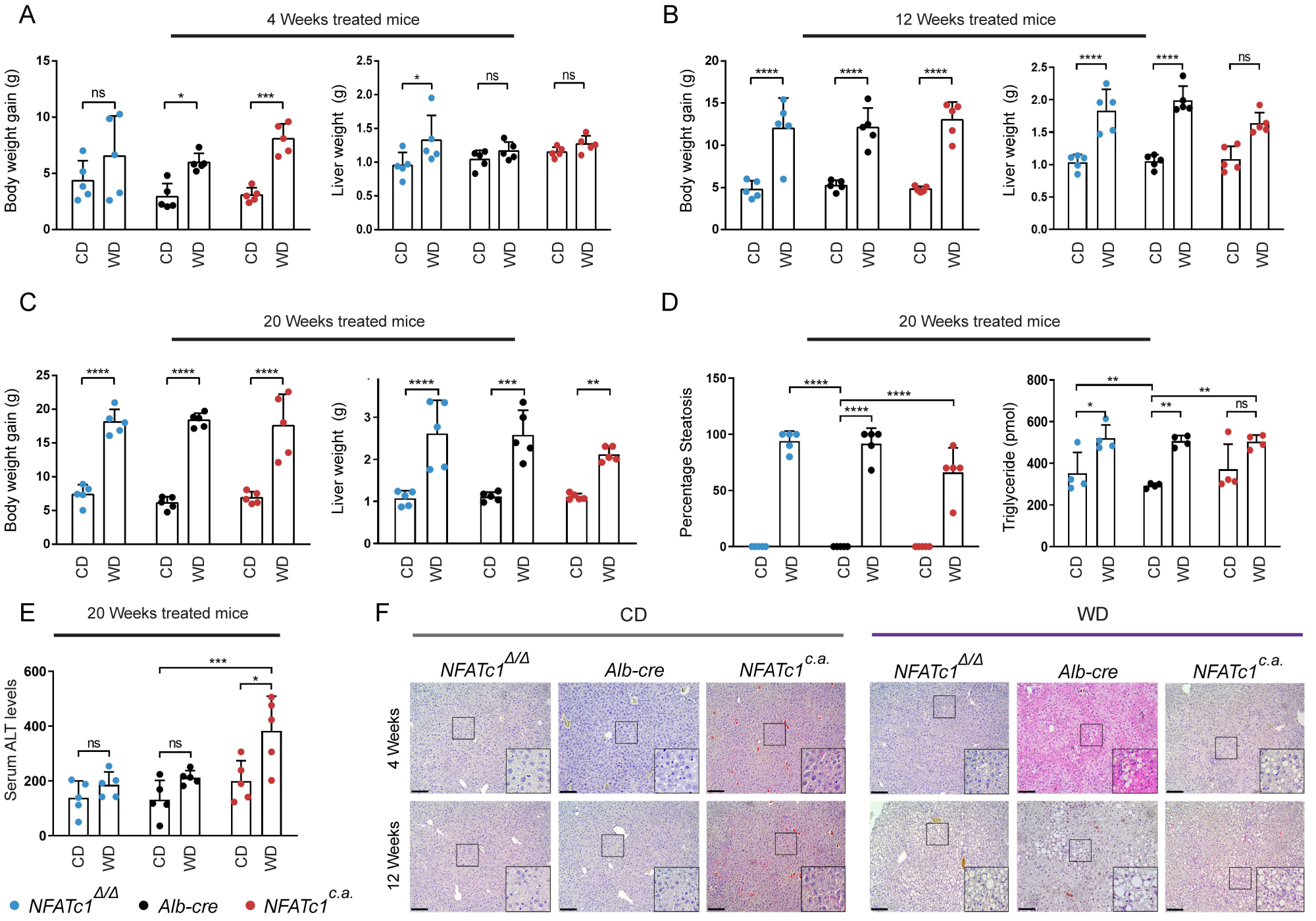
A
4 Weeks treated mice
Body weight gain (g)
Liver weight (g)
B
12 Weeks treated mice
C
20 Weeks treated mice
D
20 Weeks treated mice
Percentage Steatosis
Triglyceride (pmol)
E
20 Weeks treated mice
Serum ALT levels
NFATc1Δ/Δ
Alb-cre
NFATc1c.a.
F
CD
WD
4 Weeks
12 Weeks

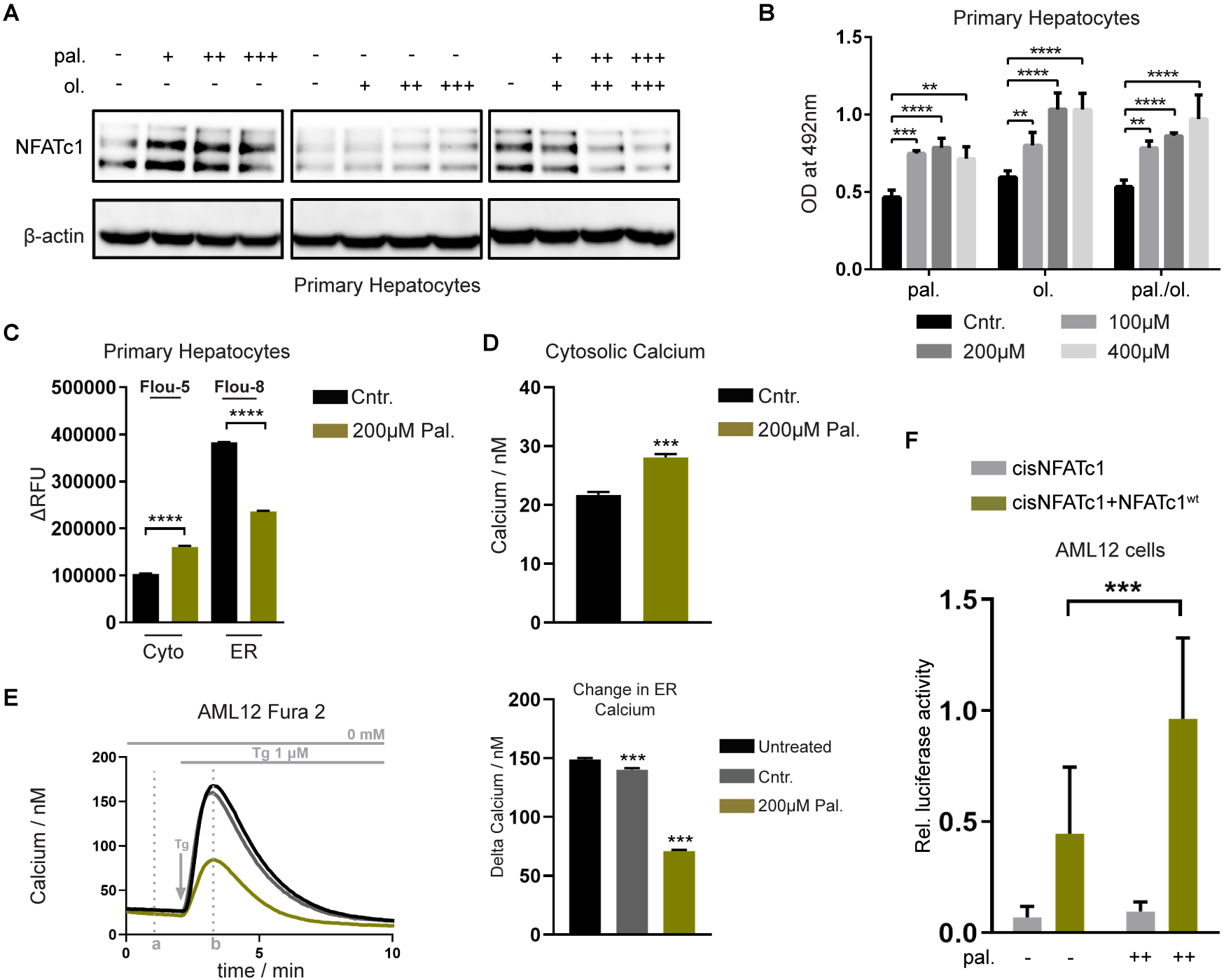
A
pal. - + ++ +++ - - - - + ++ +++
ol. - - - - - + ++ +++ - + ++ +++
NFATc1
β-actin
Primary Hepatocytes
B
Primary Hepatocytes
OD at 492nm
1.5
1.0
0.5
0.0
pal.
ol.
pal./ol.
Cntr.
100μM
200μM
400μM
C
Primary Hepatocytes
ΔRFU
500000
400000
300000
200000
100000
0
Flou-5
Flou-8
Cntr.
200μM Pal.
Cyto
ER
D
Cytosolic Calcium
Calcium / nM
40
30
20
10
0
Cntr.
200μM Pal.
Change in ER Calcium
Delta Calcium / nM
200
150
100
50
0
Untreated
Cntr.
200μM Pal.
E
AML12 Fura 2
Calcium / nM
0 mM
Tg 1 μM
Tg
a
b
time / min
F
cisNFATc1
cisNFATc1+NFATc1wt
AML12 cells
Rel. luciferase activity
1.5
1.0
0.5
0.0
pal. - - ++ ++

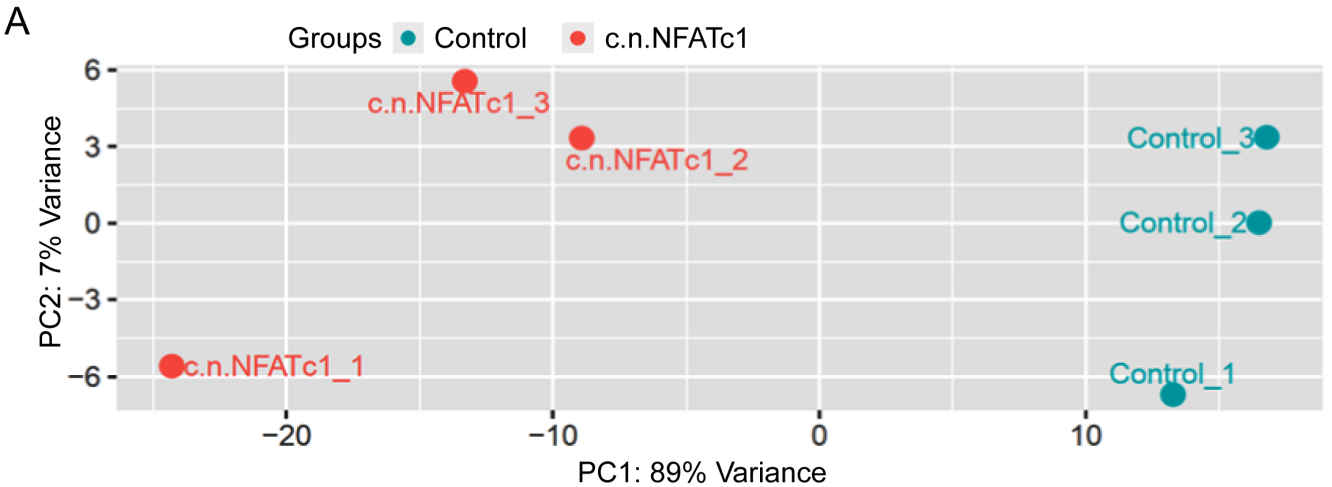
A
Groups Control c.n.NFATc1
c.n.NFATc1_3
c.n.NFATc1_2
c.n.NFATc1_1
Control_3
Control_2
Control_1
PC2: 7% Variance
PC1: 89% Variance

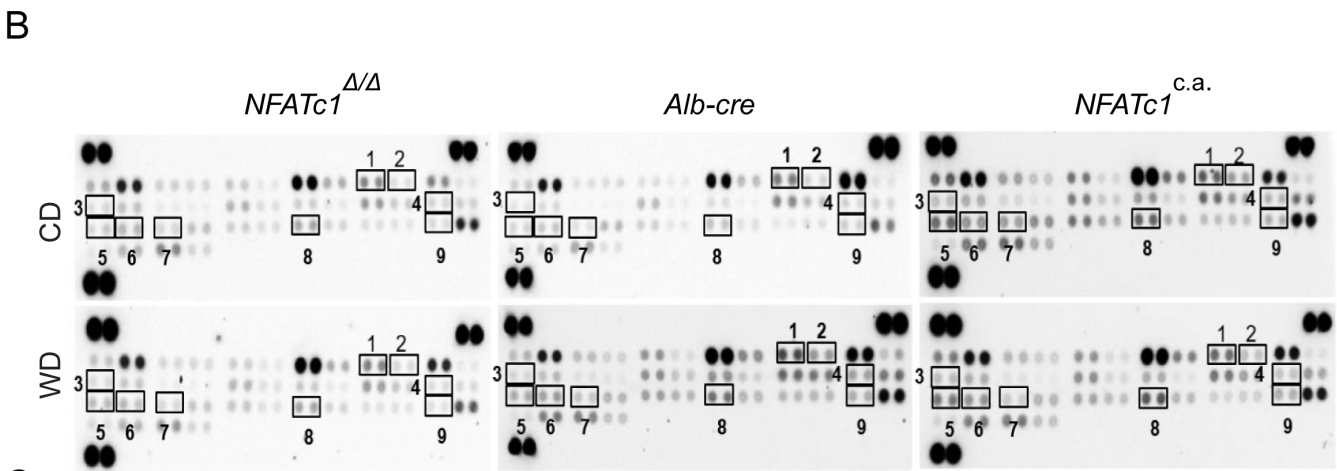
B
NFATc1Δ/Δ
Alb-cre
NFATc1c.a.
CD
WD

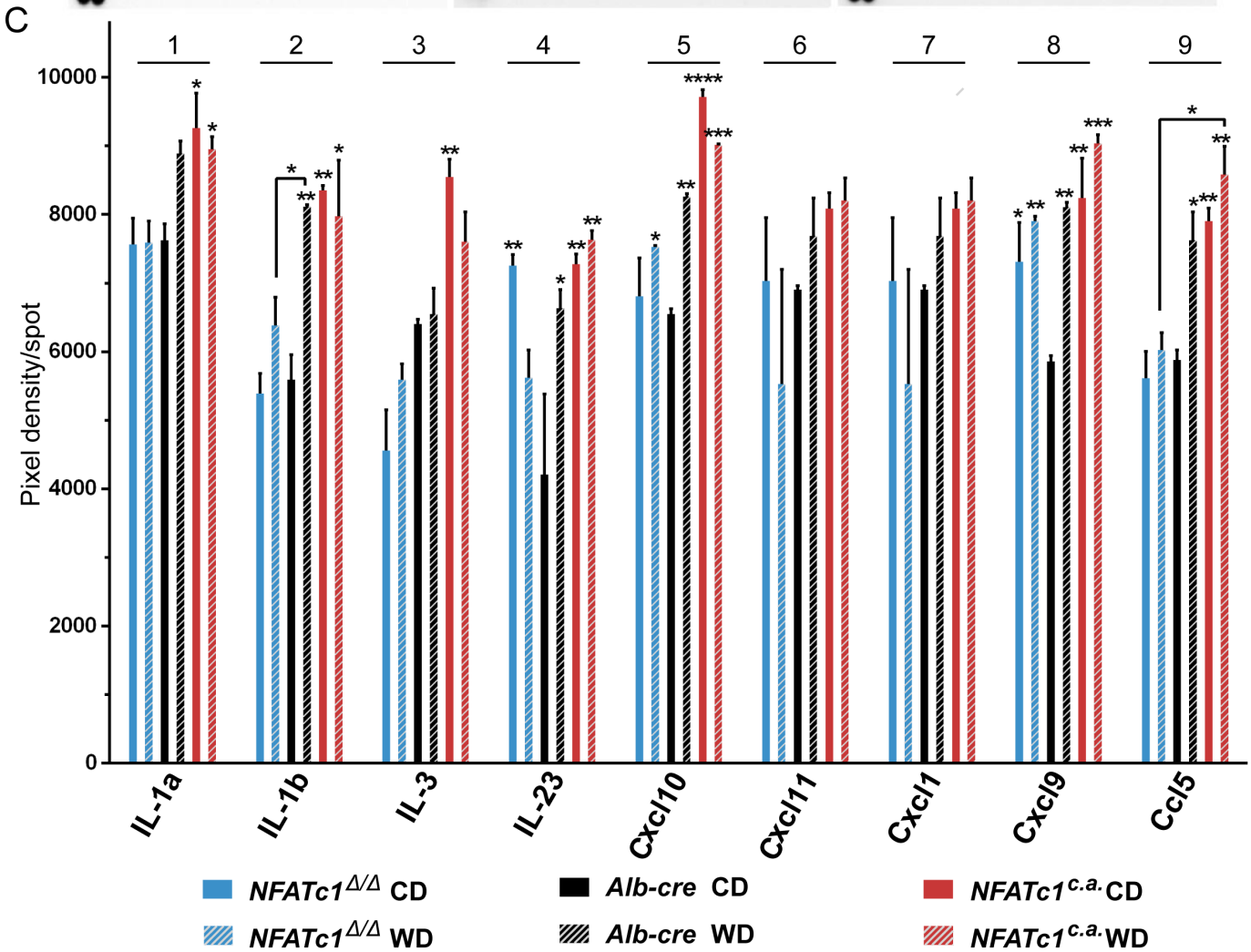
C
Pixel density/spot
IL-1a
IL-1b
IL-3
IL-23
Cxcl10
Cxcl11
Cxcl1
Cxcl9
Ccl5
NFATc1Δ/Δ CD
NFATc1Δ/Δ WD
Alb-cre CD
Alb-cre WD
NFATc1c.a. CD
NFATc1c.a. WD

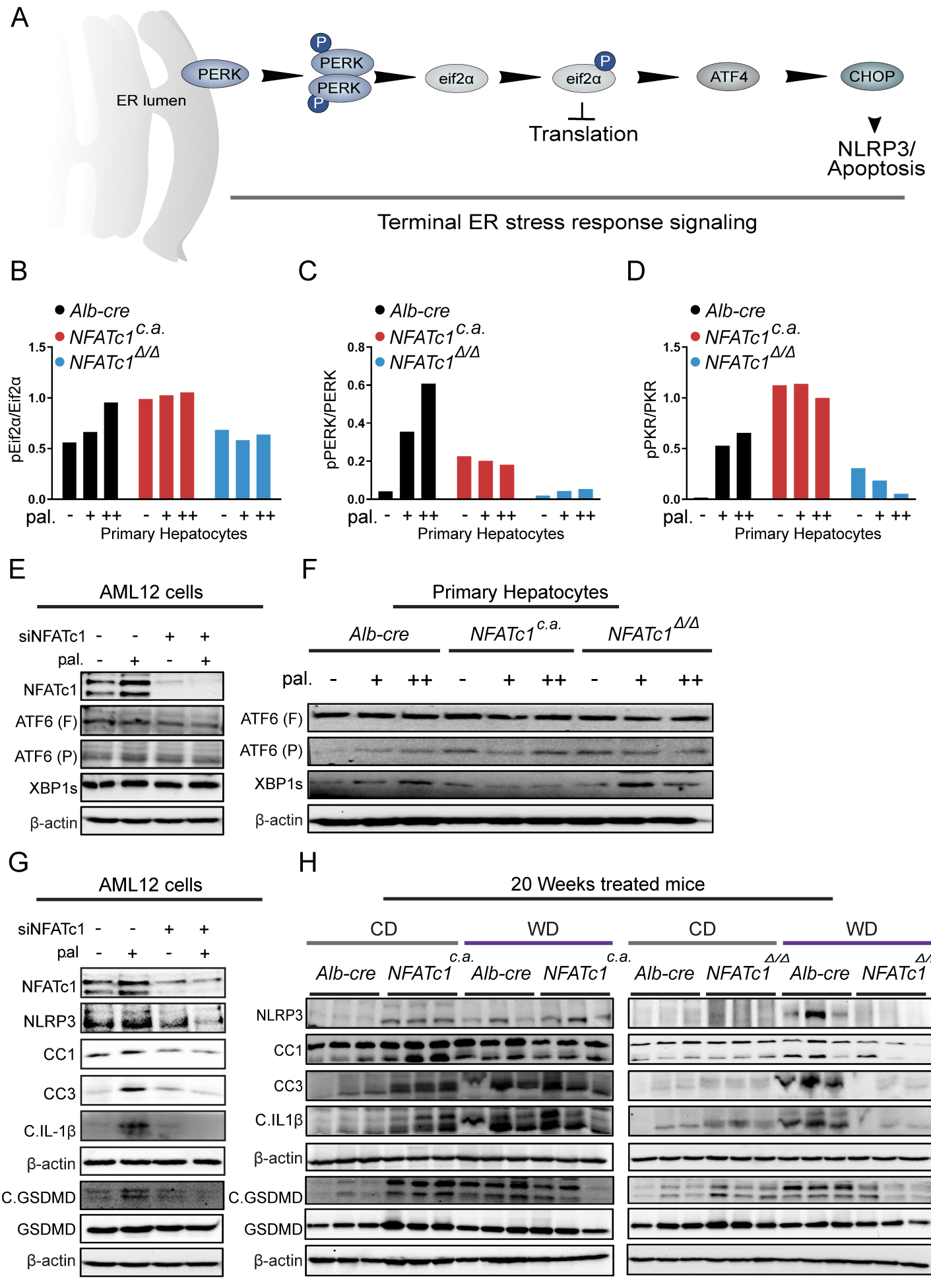
A
ER lumen
PERK
PERK
PERK
eif2α
eif2α
ATF4
CHOP
Translation
NLRP3/
Apoptosis
Terminal ER stress response signaling
B
Alb-cre
NFATc1c.a.
NFATc1Δ/Δ
pEif2α/Eif2α
pal. - + ++ - + ++ - + ++
Primary Hepatocytes
C
pPERK/PERK
D
pPKR/PKR
E
AML12 cells
siNFATc1
pal.
NFATc1
ATF6 (F)
ATF6 (P)
XBP1s
β-actin
F
Primary Hepatocytes
G
AML12 cells
C.IL-1β
C.GSDMD
GSDMD
H
20 Weeks treated mice
CD
WD
NLRP3
CC1
CC3
C.IL1β

A

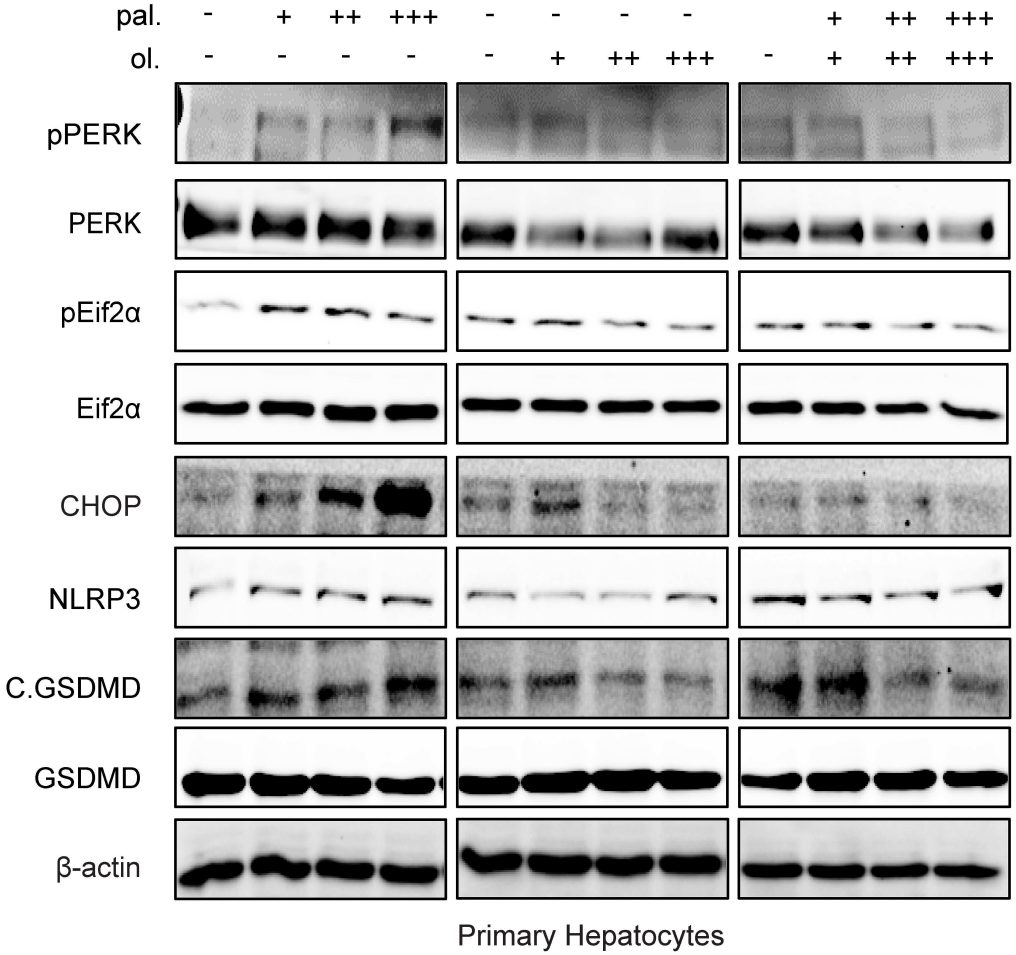
pal. - + ++ +++ - - - - + ++ +++
ol. - - - - - + ++ +++ - + ++ +++
pPERK
PERK
pEif2α
Eif2α
CHOP
NLRP3
C.GSDMD
GSDMD
β-actin
Primary Hepatocytes

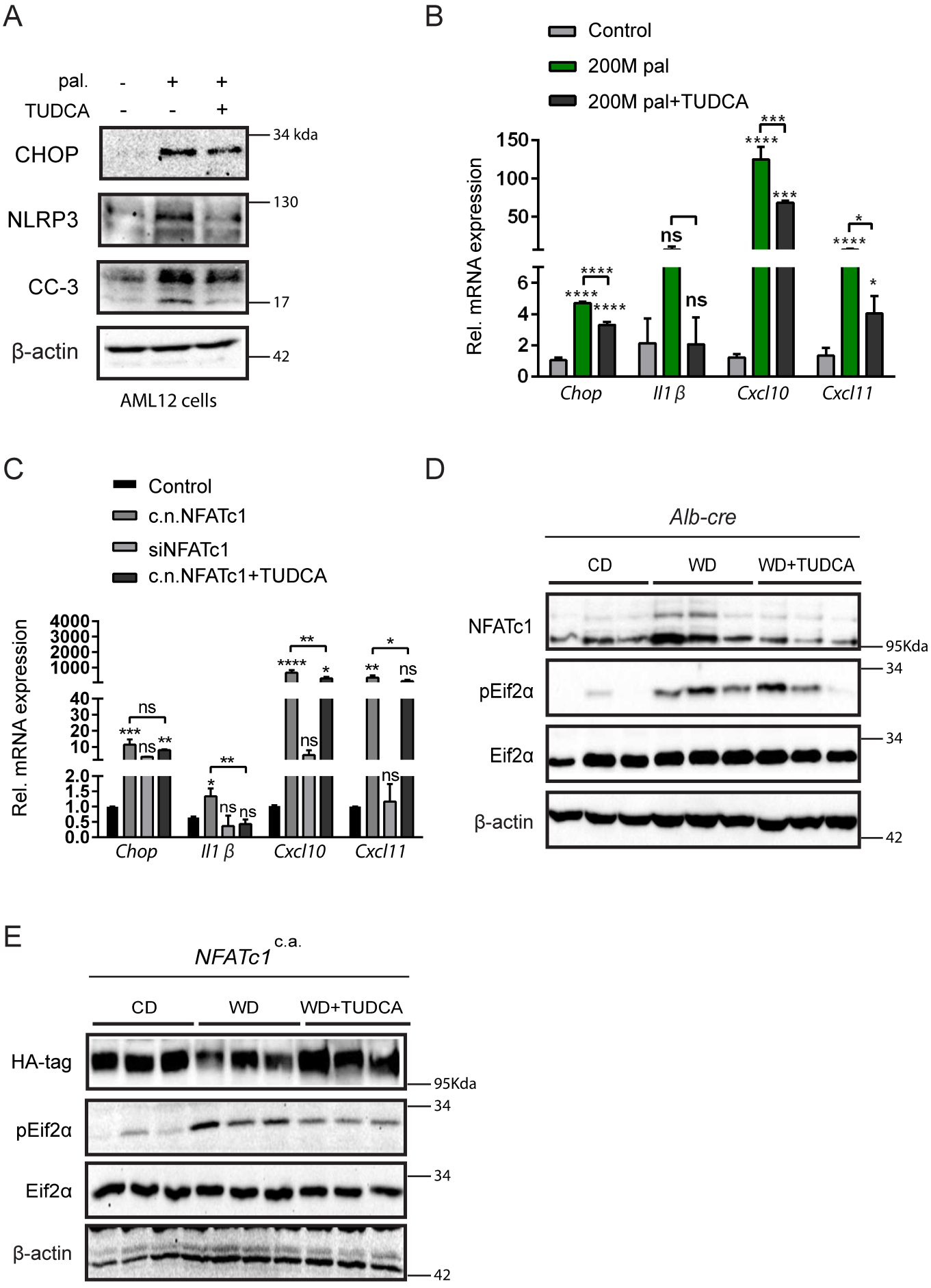
A
pal. - + +
TUDCA - - +
CHOP
NLRP3
CC-3
β-actin
34 kda
130
17
42
AML12 cells
B
Control
200M pal
200M pal+TUDCA
Rel. mRNA expression
Chop
Il1β
Cxcl10
Cxcl11
C
Control
c.n.NFATc1
siNFATc1
c.n.NFATc1+TUDCA
Rel. mRNA expression
Chop
Il1β
Cxcl10
Cxcl11
D
Alb-cre
CD
WD
WD+TUDCA
NFATc1
pEif2α
Eif2α
β-actin
95Kda
34
34
42
E
NFATc1 c.a.
CD
WD
WD+TUDCA
HA-tag
pEif2α
Eif2α
β-actin
95Kda
34
34
42

NFATc1 signaling drives chronic ER stress responses to promote NAFLD progression

Muhammad Umair Latif[1], Geske Elisabeth Schmidt[1], Sercan Mercan[1], Raza Rehman[2], Christine Gibhardt[5], Ioana Stejerean-Todoran[5], Kristina Reutlinger[1], Elisabeth Hessmann[1], Shiv K. Singh[1], Abdul Moeed[4], Abdul Rehman[6], Umer Javed Butt[7], Hannibal Bohnenberger[3], Philipp Stroebel[3], Sebastian Bremer[1], Albrecht Neesse[1], Ivan Bogeski[5], Volker Ellenrieder[1]

[1]Department of Gastroenterology, Gastrointestinal Oncology and Endocrinology, University Medical Center, Goettingen, Germany; [2]Gastrointestinal unit, Massachusetts General hospital, Harvard Medical school, USA; [3]Institute for Pathology, University Medical Center Goettingen, Germany; [4]Institute for Microbiology and Hygiene, University Medical Center Freiburg, Germany; [5]Molecular Physiology, Institute of Cardiovascular Physiology, University Medical Center, Goettingen, Germany; [6]Institute of Pharmacology and Toxicology, University Medical Center, Goettingen, Germany; [7]Clinical Neuroscience, Max-Planck Institute for Experimental Medicine.

Corresponding author

Correspondence to Prof. Dr. Volker Ellenrieder, Department of Gastroenterology, Gastrointestinal Oncology and Endocrinology, Robert-Koch Strasse 40, 37075, Goettingen, Germany; volker.ellenrieder@med.uni-goettingen.de.

Latif MU, *et al. Gut* 2022;0:1–13. doi: 10.1136/gutjnl-2021-325013

Materials and Methods

Animal care and Treatments

Mice breeding was performed in the Central Animal Facility of the University Medical Center, Goettingen. Mice were kept under controlled atmosphere in 12 hours light and dark cycles with *ad libitum* supply of food and water. Mice were caged separately based upon gender, treatment, and genotype, and housed in the same facility. At the age of 8 weeks, mice (n=5/group, following RRR principle) were randomly subjected to the different experimental protocols as follows: A) mice of all genotypes were fed with either control diet (CD) or high-fat/high-cholesterol western diet (WD) (ssniff Spezialdiäten GmbH, E15721-347) with 45% (w/w) glucose (Merck) and 55% (w/w) fructose (Carl Roth GmbH) in water) for 4, 12 and 20 weeks. B) *Alb-cre* and *NFATc1*$^{c.a.}$ mice were fed with CD or WD for 20 weeks, and WD treatment was combined with i.p. injections 3x/week of either TUDCA (Merck Millipore) (500 mg/kg of body weight) or vehicle (PBS), respectively. During treatment phase, body weight was recorded once a week. Upon completion of treatment time points liver tissues and blood samples were collected for molecular, histological and serological analysis. Investigators were unaware of allocation of experimental groups and analysis performed. Animal experiments were reported using ARRIVE1 reporting guidelines.

Cell Culture

The alpha mouse liver-12 (AML12, ATCC CRL-2254) cells were cultured at 37 °C with 5% CO_2 in Dulbecco's Modified Eagle Medium (DMEM)/Nutrient Mixture F-12 (1:1) supplemented with 10% (v/v) FBS (Biowest S181B-500), 40 ng/ml dexamethasone (Sigma-Aldrich, USA) and 1% (v/v) of Insulin-Transferrin-Selenium-Ethanolamine (100X) (Life Technologies 51500-056). At 90% confluency, cells were washed with PBS followed by trypsinization (Gibco, 15400-54 1:10 in PBS). Primary mouse hepatocytes were isolated from 8 weeks old *Alb-cre, NFATc1*$^{c.a.}$ and *NFATc1* $^{\Delta/\Delta}$ mice by two-step collagenase perfusion, as described before [1]. Isolated hepatocytes were maintained in attachment medium (Williams Medium E (1x), Gibco-22551-022, supplemented with 10% (v/v) FBS, 100nM dexamethasone, 2mM L-Glutamine (Sigma-Aldrich, USA) and 1% (v/v) Penicillin/streptomycin (Sigma-Aldrich, USA)) and seeded in 6 well plates (1 million cells/well) followed by incubation at 37 °C with 5% CO_2. After 6 hours incubation, cells were washed with PBS and medium was exchanged with pre-starvation medium (Williams Medium E (1x), supplemented with 100nM dexamethasone, 2mM L-Glutamine and 1% Penicillin/streptomycin) followed by overnight incubation. The following day, plates were washed twice with PBS and cells were provided starvation medium (Williams Medium E (1x) supplemented with 2mM L-Glutamine and 1% Penicillin/streptomycin) and maintained at similar conditions. Following experimental procedures were carried out in cells:

Latif MU, *et al. Gut* 2022;0:1–13. doi: 10.1136/gutjnl-2021-325013

i) Transfection

AML12 cells were transfected for 24 hours with *Nfatc1* siRNA (ambion 288360) or with constitutively active *Nfatc1* construct (HA-tagged MSCV- caNFATc1 bearing Serine to Alanine mutation in conserved serine rich residues). Control cells were treated with lipofectamine 2000 (Invitrogen) as vehicle. Cells were seeded and allowed to grow until 60% confluency. siRNA and c.n.NFATc1 construct were prepared in serum-free media with lipofectamine 2000, respectively.

ii) Fatty acids treatment

AML12 cells were exposed to 200 µM palmitate supplemented in medium for 12 hours. In another approach, AML12 cells were transfected for 24 hours with siRNA for *Nfatc1* or with lipofectamine 2000. After 12 hours of transfection 200 µM palmitate was added in the medium and cells were incubated for next 12 hours. Primary mouse hepatocytes were treated with 100, 200 and 400 µM of either palmitate and oleate alone or in combination, respectively for 12 hours, provided in starvation medium. Control cells were provided BSA.

iii) TUDCA Treatment

AML12 cells were seeded and treated on the following day, fresh medium containing either BSA and H_2O or 200µM Palmitate with 500µM TUDCA was provided for 12 hours [2]. In another approach, AML12 cells were pre-transfected with c.n.NFATc1 construct for 24 hrs. Following 12 hours of transfection, medium containing H_2O/TUDCA (500 µM) was added for next 12 hours. Primary mouse hepatocytes were treated with 200 µM palmitate alone, and in combination with increasing concentrations of TUDCA i.e., 100 µM-500 µM respectively, for 12 hours, provided in starvation medium. Control cells were provided BSA along with H_2O as vehicle control for TUDCA.

Reporter Assay

Dual luciferase reporter gene assay was performed in AML12 cells and primary mouse hepatocytes to verify palmitate induced transcriptional activation of NFATc1. Cells were co-transfected with a NFAT responsive promoter luciferase reporter construct in combination with either an empty vector or a NFATc1 wild-type expression vector, and subsequently treated with 200 µM palmitate (pal) for 24 hours. Renilla luciferase was used as an internal control for transfection efficiency and normalization. Promoter activity is shown as relative firefly luciferase activity normalized to renilla luciferase activity.

Measurement of cytosolic and ER Calcium concentrations

AML12 cells, seeded on 25 mm round (No 1.5, #6310172, VWR) glass coverslips, were loaded with 1 µM Fura-2 AM (#F1221, Thermo Fisher Scientific GmbH) in growth medium for 30 minutes at room temperature. The measurements were performed at room temperature in

Ringer's buffer (pH 7.4) containing 145 mM NaCl, 4 mM KCl, 10 mM Glucose, 10 mM HEPES (4-(2-hydroxyethyl)-1-piperazineethanesulfonic acid), 2 mM $MgCl_2$ and 0.5 mM $CaCl_2$, or 0 mM $CaCl_2$ with 1 mM EGTA as indicated in the figure legends. Fura-2-based measurements of cytosolic calcium were performed using a Zeiss Axiovert S100TV equipped with a pE-340_{fura} (CoolLED, Andover, United Kingdom) LED light source with LED 340 nm (excitation filter: 340/20) and 380 nm (excitation filter: 380/20) together with a T400 LP dichroic mirror and 515/80 emission filter, a sCMOS pco.edge camera and a Fluar 20x/0.75 objective. AML12 cells were treated with 200 µM palmitate for the indicated time points and basal cytosolic calcium levels were measured in Ringer's buffer containing 0.5 mM calcium. Depletion of ER calcium stores was measured in calcium free Ringer's buffer and depletion of ER stores was achieved by addition of Thapsigargin (Tg, 1 µM) using a perfusion system in untreated cells or cells treated for 12 hours with BSA and 200 µM palmitate. Data were analyzed with VisiView® Software (Visitron Systems GmbH, Puchheim, Germany). The obtained 340 nm/ 380 nm fluorescence ratios were converted to calibrated data using the equation $[Ca^{2+}] = K^*(R - R_{min})/(R_{max} - R)$, while the values of K, R_{min}, and R_{max} were determined as described previously [3].

For primary hepatocytes palmitate treated cells were incubated for 30 min with cytoplasmic calcium dye Fluo-8 (K_d 389 nM). For the ER calcium, cells were loaded with Fluo-5N (K_d 90 µM). Time-lapse live-cell calcium imaging was performed in a climate chamber (37°C, 5% CO_2) using an inverted fluorescence microscope (Olympus) with GFP filter (BP 470/20). The calcium levels were represented by changes in fluorescent intensities of the cells subtracted from the background with the help of time series analyzer V 3.0 plugin of Image J and are presented as change in fluorescence units (∆RFU).

Immunoblotting, Immunohistochemistry and Immunofluorescence

Hematoxylin eosin staining, IHC and western blot analysis were performed using standard protocol as described previously [4], using antibodies against HA-tag (#3724; Cell Signaling), NFATc1 (7A6, #sc7294; Santa Cruz Biotechnologies and ab25916; abcam), CD45 (#550539; BD Pharmingen), eif2α (#9722; Cell signaling), p-Eif2α (#9721; Cell Signaling), CHOP(#2895; Cell Signaling), Ddit3 (ab179823; abcam), cleaved caspase-3 (#9661; Cell signaling), cleaved caspase-1 (#67314; Cell signaling), cleaved IL-1β (#52718; Cell signaling), pP53-(s15) (#9284; Cell signaling), NLRP3 (AG-203-0014-C101; Adipogene) and β-actin (A3845; Sigma), Gasdermin D (#39754; Cell signaling), cleaved Gasdermin D (#10137; Cell signaling); TRB3 (#LS-B12111; LSBio), ATF4 (#NB100-852; Novusbio), PERK (#3192; Cell signaling), p-PERK (#3179; Cell signaling), p-PKR (#MBS856680; MyBioSource), PKR (#MBS150276; MyBioSource). For immunoblot analysis of animal tissues each lane represents an individual mouse. For immunostaining and immunofluorescence, scale bar of images are 100 and 200

µm respectively, unless stated differently. For quantification of IHC and IF imageJ software was utilized. For NFATc1 IHC, percentage of NFATc1 positive hepatocytes to a total number of cells was calculated by manual quantification. Percentage of CD45 positive cells were quantified in imageJ using semi-automatic macros. To analyze the fibrosis liver tissue sections were stained with picrosirius red according to the manufacturer's protocol (Polysciences, Inc). For collagen counting percentage of picrosirius red stained area was quantified.

Oil-Red-O staining

Oil red o staining was performed in primary mouse hepatocytes and in liver sections from 20 weeks CD and WD treated mice, respectively, as per manufacturer's instructions (#O1391; Sigma). Briefly, primary hepatocytes were pretreated with 100, 200 and 400 µM of either palmitate and oleate alone or in combination for 12 hours. Later, cells were fixed in 4% paraformaldehyde and stained with oil-red-o. Cells were incubated in 100% isopropanol for 5 mins and OD was measured at 492nm. For mice, 4 µm thick cryosections were stained with oil red o.

RNA isolation and real-time PCR (qRT-PCR)

RNA isolation was performed using phenol-chloroform purification and cDNA was synthesized using iScript cDNA Synthesis Kit (170-8891, BioRad,) as described before [4 5]. mRNA expression analysis for each sample was performed in triplicates using iTaq Universal SYBR Green Supermix (BioRad, 172-5125) with StepOne Plus Real-Time PCR System (Applied Biosystems). Gene expression values for each sample were normalized to housekeeping gene *Gapdh* and compared to control. Graphical representation and statistical analysis of results was performed in GraphPad Prism, version 9.0. Statistical significance and its method are described in respective results.

Cytokine profiling

Snap-frozen liver tissues from CD and WD treated mice were analysed using a Proteome Profiler Mouse Cytokine Array Kit (R&D Systems, Minneapolis, MN, USA). The samples were prepared as per manufacturer's protocol. The densitometric volume was determined by imageJ software. All the experimental procedures were performed strictly following manufacturers' instructions.

Triglyceride Assay

Liver triglyceride content in 20 weeks CD and Wd treated mice was analysed using a fluorimetric quantification assay (#ab178780; Abcam) according to the manufacturer's instructions. Briefly, lysates from 10 mg liver tissue samples were prepared. These lysates were incubated with lipase at 37 °C for 20 mins. Reaction mix was added, and the samples

were incubated for 30 mins at 37°C. The absorbance was recorded at E_x/E_m = 535/587 nm using a microplate reader.

Chemicals and preparations

Palmitate **(**Sigma Aldrich, 408-35-5**)** and Oleate (Sigma Aldrich, O7501-5G) were dissolved in 150 mM NaCl in conjugation with BSA (Serva, 9048-46-8) with final ratio of 1:6. Briefly, BSA was dissolved in NaCl, to prepare 0.34 mM BSA solution. Half of the BSA was diluted with 150 mM NaCl to make final concentration of 0.17 mM and filtered, for subsequent use as vehicle. 4.4 mM of sodium palmitate and sodium oleate solutions were prepared in 50 ml of 150 mM NaCl, by heating up to 70 °C and 44 ml was transferred to 0.34 mM BSA solution already prepared following stirring at 37 °C for 1 hour. After adjusting pH 7.4, final volume was raised up to 100 ml with 150mM NaCl, to make final concentration 2mM. Palmitate/BSA and oleate/BSA solutions were filtered and stored at -20 °C. Tauroursodeoxycholic Acid (TUDCA, Millipore 580549) was solved in H_2O (20 mM), filtered, and stored at 4 °C for further experiments. For i.p. injections in mice TUDCA was dissolved in PBS at final concentration of 500mg/kg body weight.

Statistical analysis

Statistical analysis was perfomed by Graphpad Prism 9.0 using unpaired t-test, one-way ANOVA and two-way ANOVA, respectively (described in each figure legend). Grubb's test was used to identify the statically significant outlier. Statistical significance was always mentioned as *p <0.05, **p <0.005, ***p< 0.0005, ****p<0.0001.

Supplementary Figure legends

Supplementary Figure 1

Graphs presenting analysis of changes in body weight and liver weight after (A) 4 weeks, (B) 12 weeks and (C) 20 weeks of CD and WD treatment (n=5). (D) Graphs show qualitative analysis of percentage steatosis (n=5), and the liver triglyceride levels (n=4) in 20 weeks CD and WD treated mice. (E) Quantification of serum ALT values in *NFATc1*$^{\Delta/\Delta}$, *Alb-Cre* and *NFATc1*$^{c.a.}$ mice treated with CD and WD for 20 weeks (n=5). Statistical analysis (A-E) was performed by Two-way ANOVA and data are shown as mean ± SD, *p*-values are *p<0.05, **p< 0.005, ***p<0.0005 and ****p<0.0001. (F) Representative images from H&E analysis of liver sections from 4- and 12-weeks of CD and WD treated mice (n=5). Scale bar =100 µm.

Supplementary Figure 2

(A) Western blot analysis of NFATc1 protein expression in primary mouse hepatocytes treated with 100 µM (+), 200 µM (++) and 400 µM (+++) of either palmitate (pal.) and oleate (ol.) alone or in combination (pal./ol.) for 12 hours. (B) Graph represents quantitative analysis of Oil-Red-

O staining in primary mouse hepatocytes pretreated with BSA, 100, 200 and 400 µM of either palmitate (pal.) and oleate (ol.) alone or in combination (pal./ol.) for 12 hours. (C) Changes in ER and cytosolic calcium levels in palmitate (200 µM) treated primary hepatocytes were measured using ER calcium specific Fluo-5N (K_d 90 µM) and cytoplasmic calcium specific dye Fluo-8 (K_d 389 nM). The changes in calcium levels are represented as change in fluorescence units (∆RFU). (D) Cytosolic calcium levels were measured in AML-12 cells using Fura-2 in Ringer's buffer containing 0.5 mM calcium after treatment with 200 µM palmitate for 12 hours. (n values: untreated= 919 cells, 200µM Palmitate=726 cells, N=3). (E) Calcium release from internal ER stores was measured in calcium free Ringer's buffer upon administration of thapsigargin (Tg 1µM) in AML-12 cells using Fura-2-based calcium imaging. Cells were pre-treated for 12 hours with 200µM palmitate. Graph represents quantification of Tg-induced ER calcium store release ((b)-(a)). (n values: untreated= 1537 cells, BSA control=1067 cells, 200 µM palmitate=1491 cells, from 3 independent experiments). (F) Dual luciferase reporter gene assay was performed in AML12 cells to verify palmitate induced transcriptional activation of NFATc1. Cells were co-transfected with a NFAT responsive promoter luciferase reporter construct in combination with either an empty vector or a NFATc1 wild-type ($NFATc1^{wt}$) expression vector, and subsequently treated with 200 µM palmitate (pal.) for 24 hours. Statistical analysis was performed by Two-way ANOVA (B), One-way ANOVA (C, E-F) by unpaired t-test (D). Data are shown as mean ± SD, $*p< 0.05$ and $**p< 0.005$, $***p< 0.0005$ and $****p< 0.0001$.

Supplementary Figure 3

(A) Principal component analysis showing differential clustering replicates per groups. (B) Cytokine proteome profiling in liver tissue lysates of 20 weeks treated genetic mice. (n=3) (C) Quantitative analysis of cytokine proteome profiling. Statistical analysis was performed by paired t-test. Data are shown in mean ± SD, p-values are $*p < 0.05$, $**p< 0.005$, $***p< 0.0005$, $****p< 0.0001$. Statistical analysis was performed by two-way ANOVA.

Supplementary Figure 4

Schematic representation of ER stress induced PERK-CHOP UPR signaling. (B-D) Densitometry graphs of primary hepatocytes following 12 hours palmitate treatment (+ = 100 µM, ++ = 200 µM) for (B) pEif2α/Eif2 α, (C) pPERK/PERK and (D) pPKR/PKR. (E) Immunoblot analysis of NFATc1, ATF6 F (full length), ATF6 P (partial) and XBP1s (spliced) in AML12 cells following 12 hours palmitate treatment (+ = 200 µM) alone or in combination with siNFATc1. (F) Protein levels of ATF6 F (full length), ATF6 P (partial) and XBP1s (spliced) were measured in 12 hours palmitate treated primary mouse hepatocytes (+ = 100 µM and ++ = 200 µM). (G-H) Immunoblot analysis of NFATc1, NLRP3, CC-1, CC-3, C.IL1β, C.GSDMD and GSDMD in (G) AML12 cells treated with palmitate (+ = 200 µM) alone or in combination with siNFATc1 and in (H) in liver tissue lysates from 20 weeks CD and WD treated mice with differential NFATC1 expression.

Supplementary Figure 5

(A) Immunoblot examination showing protein levels of pPERK, PERK, p-Eif2α, Eif2α, CHOP, NLRP3, C.GSDMD and GSDMD (Gasdermin D) in primary mouse hepatocytes following 12

hours of 100 µM (+), 200 µM (++) and 400 µM (+++) of either palmitate or oleate alone and in combination.

Supplementary Figure 6

(A) Immunoblot analyses showing protein expression of CHOP, NLRP3 and CC-3 in AML12 cells treated with palmitate (pal., 200 µM) alone or along with TUDCA (500 µM) in comparison to control treated cells. (B-C) qRT-PCR analysis of *Chop, IL-1β, Cxcl10 and Cxcl11* in AML12 cells after exposure to palmitate alone or in combination with TUDCA (B) or following transfection with siNFATc1 and c.a. NFATc1 alone or in combination with TUDCA (C). Protein levels of NFATc1, pEif2α and Eif2α were examined in liver tissue lysates of 20 weeks CD, WD and WD+TUDCA treated (C) *Alb-cre* and (D) *NFATc1*$^{c.a.}$ mice. Each lane represents individual mouse. Data are shown in mean ± SD, p-values are **p*<0.05, ***p*<0.005, ****p*<0.0005, *****p*<0.0001. Statistical analysis was performed by one-way ANOVA.

References

1. Severgnini M, Sherman J, Sehgal A*, et al.* A rapid two-step method for isolation of functional primary mouse hepatocytes: cell characterization and asialoglycoprotein receptor based assay development. *Cytotechnology* 2012;64:187-95.
2. Nakagawa H, Umemura A, Taniguchi K*, et al.* ER stress cooperates with hypernutrition to trigger TNF-dependent spontaneous HCC development. *Cancer Cell* 2014;26:331-43.
3. Grynkiewicz G, Poenie M, Tsien RY. A new generation of Ca2+ indicators with greatly improved fluorescence properties. *J Biol Chem* 1985;260:3440-50.
4. Hasselluhn MC, Schmidt GE, Ellenrieder V*, et al.* Aberrant NFATc1 signaling counteracts TGFβ-mediated growth arrest and apoptosis induction in pancreatic cancer progression. *Cell death & disease* 2019;10:1-14.
5. Du M, Wang X, Yuan L*, et al.* Targeting NFATc4 attenuates non-alcoholic steatohepatitis in mice. *J Hepatol* 2020;73:1333-46.